AGU PUBLICATIONS

JGR

Journal of Geophysical Research: Biogeosciences

RESEARCH ARTICLE
10.1002/2013JG002597

Key Points:
- The dynamics of spruce beetle disturbance takes years from attack to mortality
- Conductance and evapotranspiration decline dramatically from blue-stain fungus
- CO2 flux is restricted after beetle attack then plummets with spruce mortality

Supporting Information:
- Readme
- Text S1
- Text S2
- Text S3
- Figure S1
- Figure S2
- Figure S3
- Table S1
- Table S2
- Table S3
- Table S4

Correspondence to:
J. M. Frank,
jfrank@fs.fed.us

Citation:
Frank, J. M., W. J. Massman, B. E. Ewers, L. S. Huckaby, and J. F. Negrón (2014), Ecosystem CO_2/H_2O fluxes are explained by hydraulically limited gas exchange during tree mortality from spruce bark beetles, *J. Geophys. Res. Biogeosci.*, *119*, 1195–1215, doi:10.1002/2013JG002597.

Received 13 DEC 2013
Accepted 25 APR 2014
Accepted article online 2 MAY 2014
Published online 19 JUN 2014

Ecosystem CO_2/H_2O fluxes are explained by hydraulically limited gas exchange during tree mortality from spruce bark beetles

John M. Frank[1,2], William J. Massman[1], Brent E. Ewers[2], Laurie S. Huckaby[1], and José F. Negrón[1]

[1]Rocky Mountain Research Station, U.S. Forest Service, Fort Collins, Colorado, USA, [2]Department of Botany and Program in Ecology, University of Wyoming, Laramie, Wyoming, USA

Abstract Disturbances are increasing globally due to anthropogenic changes in land use and climate. This study determines whether a disturbance that affects the physiology of individual trees can be used to predict the response of the ecosystem by weighing two competing hypothesis at annual time scales: (a) changes in ecosystem fluxes are proportional to observable patterns of mortality or (b) to explain ecosystem fluxes the physiology of dying trees must also be incorporated. We evaluate these hypotheses by analyzing 6 years of eddy covariance flux data collected throughout the progression of a spruce beetle (*Dendroctonus rufipennis*) epidemic in a Wyoming Engelmann spruce (*Picea engelmannii*)–subalpine fir (*Abies lasiocarpa*) forest and testing for changes in canopy conductance (g_c), evapotranspiration (ET), and net ecosystem exchange (NEE) of CO_2. We predict from these hypotheses that (a) g_c, ET, and NEE all diminish (decrease in absolute magnitude) as trees die or (b) that (1) g_c and ET decline as trees are attacked (hydraulic failure from beetle-associated blue-stain fungi) and (2) NEE diminishes both as trees are attacked (restricted gas exchange) and when they die. Ecosystem fluxes declined as the outbreak progressed and the epidemic was best described as two phases: (I) hydraulic failure caused restricted g_c, ET ($28 \pm 4\%$ decline, Bayesian posterior mean ± standard deviation), and gas exchange (NEE diminished $13 \pm 6\%$) and (II) trees died (NEE diminished $51 \pm 3\%$ with minimal further change in ET to $36 \pm 4\%$). These results support hypothesis b and suggest that model predictions of ecosystem fluxes following massive disturbances must be modified to account for changes in tree physiological controls and not simply observed mortality.

1. Introduction

Forest ecosystems are changing in response to disturbance [*Allen et al.*, 2010; *Masek et al.*, 2008; *van Mantgem et al.*, 2009]. Using physiological responses of individual plants to predict the response of an ecosystem can be challenging [*Jarvis*, 1995], requiring intensive field campaigns [*Sellers et al.*, 1997] and modeling efforts [*Mackay et al.*, 2002] to capture the relevant nonlinearities and feedbacks. Though the primary physiological response to disturbance might be obvious on the plant scale, the ultimate forest ecosystem response can be complex and difficult to predict [*Gough et al.*, 2013]. Forest ecosystems with one or two dominant trees are an ideal setting to test whether tree level physiology can be used to predict ecosystem fluxes during a mortality event, a major assumption of many ecological investigations [*Adams et al.*, 2009; *Anderegg et al.*, 2012]. In this study, we investigate disturbance in a subalpine forest to determine if known mechanisms of hydraulic failure and subsequent impacts on carbon uptake from individual trees can explain changes at the ecosystem scale.

In the Rocky Mountains of North America, bark beetles have become a major agent of change [*Raffa et al.*, 2008]. Although mountain pine beetle (*Dendroctonus ponderosae*) often grabs headlines due to 12,700,000 ha of forest affected in Canada plus another 3,300,000 ha in the western United States [*Natural Resources Canada*, 2010; *USDA Forest Service*, 2012], spruce beetle (*Dendroctonus rufipennis*) is the major insect disturbance in the subalpine spruce-fir forests of North America. Over the past two decades, spruce beetle has disrupted 1,500,000 ha of forest in Alaska [*USDA Forest Service,* 2009] and is currently infesting 166,000 ha in the western United States, with 84,000 ha in Colorado and 32,000 in Wyoming [*USDA Forest Service*, 2012]. Spruce beetle epidemics are not new to the Rocky Mountains [*Dymerski et al.*, 2001; *Love*, 1955; *McCambridge and Knight*, 1972; *Schmid and Frye*, 1977; *Veblen et al.*, 1991] but the potential for outbreaks is expected to rise under climate change [*Bentz et al.*, 2010]. A warming climate facilitates spruce beetle population growth by quickening the insect's life cycle from semivoltine to univoltine

[*Hansen and Bentz*, 2003] as well as reducing the chance of exposing larvae to their wintertime freeze-tolerance limit of −31°C [*Miller and Werner*, 1987].

Disturbances can have a profound impact on ecosystem fluxes of water [*Adams et al.*, 2012] and carbon [*Amiro et al.*, 2010]. Though a bark beetle epidemic has similarities to disturbance caused by harvest or fire where overstory is dramatically removed or destroyed, it is fundamentally different because some of the canopy along with the understory can survive relatively unharmed and then utilize the resources relinquished by the dying trees [*Veblen et al.*, 1991]. In addition to consuming phloem and girdling trees, many species of bark beetles interrupt the transpiration of water via their associated blue-stain fungi [*Paine et al.*, 1997] and thus mechanistically alter the ecosystem's use of water. This commonly results in tree mortality and a reduction of the assimilation of carbon within the disturbed ecosystem [*Brown et al.*, 2012]. For pine trees affected by mountain pine beetle, the cascade of hydraulic failure to reduced photosynthesis [*Katul et al.*, 2003] and ultimately tree mortality [*Edburg et al.*, 2012] can happen within months [*Hubbard et al.*, 2013; *Knight et al.*, 1991; *Yamaoka et al.*, 1995]. Yet this can take much longer in spruce forests [*Mast and Veblen*, 1994], possibly because spruce are among the few plants that survive without tightly regulating stomatal conductance to plant hydraulics [*Ewers et al.*, 2005].

To explain the ecosystem response of a subalpine forest to a spruce beetle epidemic, we weigh two competing hypotheses: (a) Changes in ecosystem fluxes are proportional to observable patterns of mortality or (b) to explain ecosystem fluxes, the physiology of dying trees must also be incorporated. We evaluate these hypotheses by analyzing 6 years of ecosystem carbon and water flux data and testing for changes in canopy conductance (g_c), evapotranspiration (ET), and net ecosystem exchange (NEE) of CO_2 (quantum yield of photosynthesis and maximum assimilation rate) throughout the progression of the epidemic. From hypothesis a, we predict that g_c, ET, and NEE all diminish as trees die. From hypothesis b, we predict (1) that g_c and ET decline as trees are attacked (hydraulic failure) and (2) NEE diminishes both as trees are attacked (restricted gas exchange) and when they die.

2. Materials and Methods

2.1. Site Description

This study was conducted at the Glacier Lakes Ecosystem Experiments Site (GLEES) AmeriFlux site (41°21.992'N, 106°14.397'W, 3190 m above sea level). GLEES is located in a high-elevation subalpine forest in the Rocky Mountains of southeastern Wyoming [*Musselman*, 1994]. The forest overstory reaches 18 m and is dominated by Engelmann spruce (*Picea engelmannii*) which composes 72% of the stems and 84% of the basal area while subalpine fir (*Abies lasiocarpa*) accounts for the rest (H. Speckman et al., manuscript in preparation, 2014). In recent years, the forest has experienced an outbreak of spruce beetle. Over the past two decades, wintertime low temperatures at GLEES have fallen below the spruce beetle freeze-tolerance threshold of −31°C on only three occasions (February 1989, December 1990, and February 2011; http://www.fs.fed.us/rm/data_archive/, http://ameriflux.ornl.gov/).

We used a dendrochronological survey to determine when spruce beetles were most actively attacking trees. Preliminary work was done in 2008 when seven spruces were cored near the AmeriFlux scaffold. We then established plots on a 200 m grid totaling 0.8 km × 1.2 km with the long edge oriented east–west and the eastern edge centered 200 m west of the scaffold. Of the 35 grid intersections, 29 were forested and permanently marked as a plot center. During 2009–2010, we sampled trees using the point-centered quarter method [*Cottam and Curtis*, 1956] plus trees within 8 m of the plot center that were obviously older or had visible scars. All trees were cored at 0.35 m height with an increment borer. We noted any visible evidence of spruce beetle for each tree sampled (i.e., pitch tubes). We measured age to coring height by harvesting ~0.35 m tall seedlings ($n = 12$). Samples were prepared and cross-dated using standard dendrochronological methods [*Stokes and Smiley*, 1968]. We cross-dated our samples with the Sheep Trail ring width chronology collected at GLEES (1097–1999 CE, Peter Brown, Connie Woodhouse, Malcolm Hughes, Linda Joyce, International Tree Ring Data Bank). Samples off pith by less than 20 rings were aged using the concentric circle method [*Applequist*, 1958]. Samples off pith by more than 20 rings or that were rotten were aged by multiplying radius at sampling height by the ring density inside 10 cm of the core.

We determined the temporal dynamics of beetle attacks by determining the cumulative percentage of trees that ceased wood growth in their rings. We assumed that the mortality of a tree which had obvious signs of

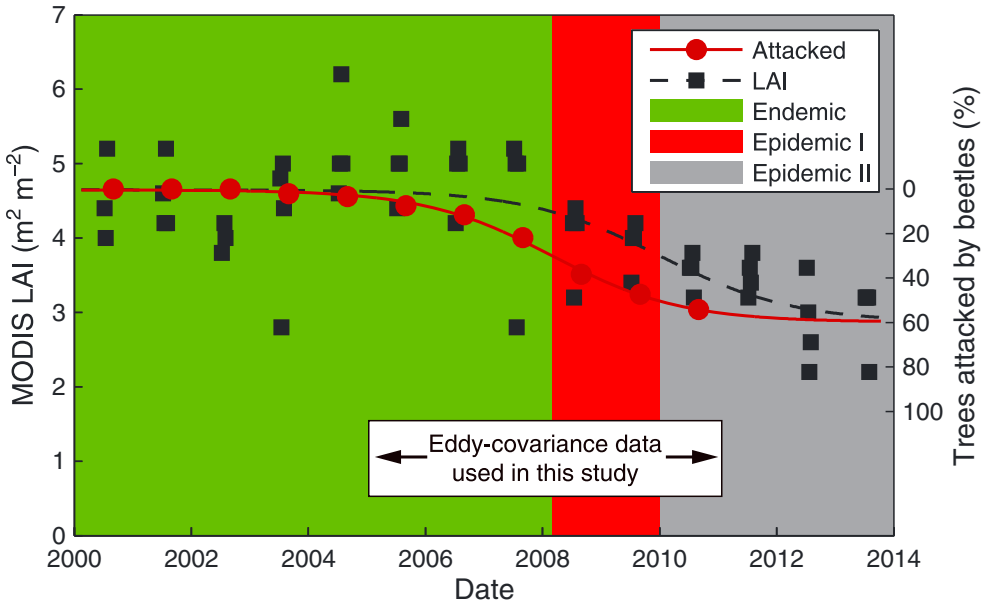

Figure 1. Temporal dynamics of when trees were attacked by beetles relative to when they died. Attacks were determined from our dendrochronological survey. Observable mortality was determined from MODIS LAI. A logistic sigmoid function (equation (1)) was fit to both data sets and estimated that the midpoint of attacks occurred in March 2008 corresponding to the transition from endemic to epidemic I. The midpoint in mortality occurred in January 2010 corresponding to the transition between epidemic I and II. The estimated difference in transition time between attacks and mortality is 1.8 ± 0.9 years, which is consistent with *Mast and Veblen* [1994] who found that tree ring production in Engelmann spruce stops 1 to 3 years before actual tree death.

elevated defenses against beetles (e.g., pitch tubes) could only be attributed to beetle attack instead of a climate-induced process such as drought stress. Based on a subset of trees that were actively under attack when sampled, we determined that most trees ceased putting on latewood between late August and early September in the year they were attacked. We determined the dynamics of when spruce trees were dying based on observable patterns of tree mortality detected by Moderate Resolution Imaging Spectroradiometer (MODIS) Terra leaf area index (LAI) [*Myneni et al.*, 2002] (https://lpdaac.usgs.gov/data_access, maintained by the NASA Land Processes Distributed Active Archive Center (LP DAAC), USGS/Earth Resources Observation and Science (EROS) Center, Sioux Falls, South Dakota, 2013) in the pixel containing the scaffold (Figure S1 in the supporting information). The MODIS LAI was seasonal with an average peak among all years on 21 July; we selected all MODIS data from 2000 to 2013 collected within ±2 weeks of this date and screened out data with the LAI quality assurance, quality control (QA/QC) flag set ($n = 54$, 4 for most years), and applied the coniferous forest multiplier of 2. We fit a logistic sigmoid function (equation (1) and Figure 1) to both the dendrochronological and MODIS data sets:

$$Y = \Delta_y \tanh\left(\frac{m(t - t_{50})}{\Delta_y}\right) + y_{50} \quad (1)$$

where Y is the response data, the predictor t is time, t_{50} is the time when half the transition in Y occurs, y_{50} and m are the value and slope of Y at the midpoint, and Δ_y is the absolute change in Y from midpoint to asymptote (SAS PROC NLMIXED, SAS Institute, Inc., Cary, NC, USA). Consistent with the values of t_{50}, we determined phases when the epidemic was characterized by either attacks or mortality. Using these results (section 3.1), the outbreak became epidemic in 2008 at which point over half of the impacted trees had been attacked (Figure 1). As a consequence, by 2010, the MODIS LAI declined 50% (Figure 1) and 73% of the spruce trees that accounted for 91% of the spruce basal area were impacted by the beetle (Speckman et al., manuscript in preparation, 2014). We classified the years 2005–2007 as endemic (characterized by some background beetle-caused tree mortality; Figure 2a), 2008–2009 as epidemic I (immediately after the peak beetle outbreak when impacted trees experience hydraulic failure; Figures 2b and 2c), and 2010 as epidemic II (impacted trees ultimately drop their green needles and die [*Mast and Veblen*, 1994]; Figure 2d).

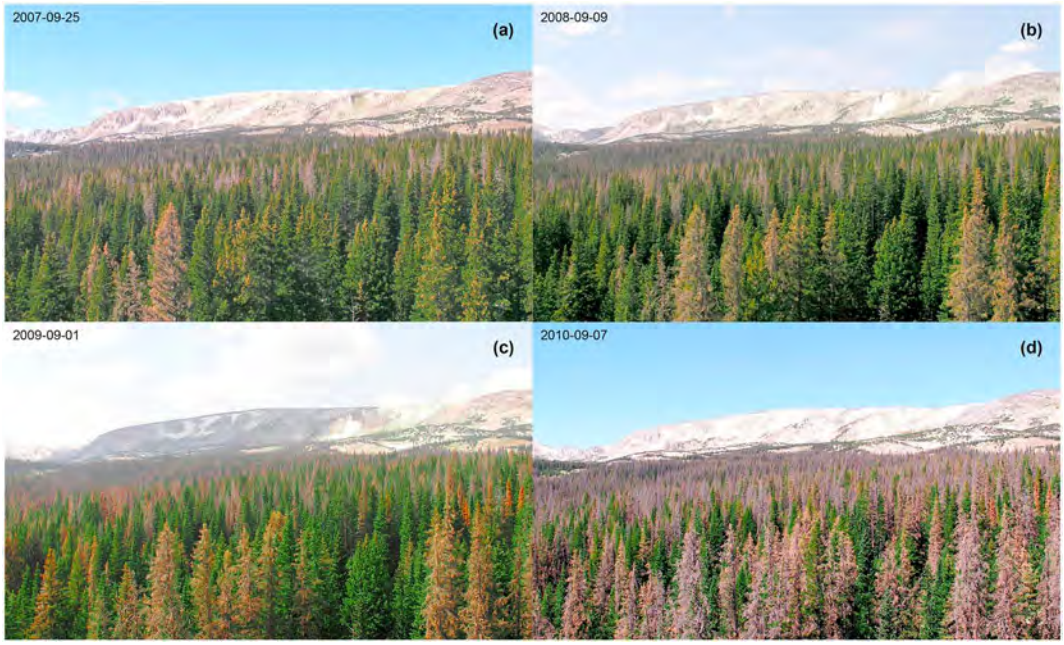

Figure 2. Repeat photography from the GLEES AmeriFlux scaffold showing the three phases of the spruce beetle outbreak: (a) endemic, (b and c) epidemic I, and (d) epidemic II.

2.2. Tree Physiology Measurements

To quantify the physiological impacts of spruce beetle/blue-stain fungi attack on spruce trees, from 2008 to 2010, five healthy and five attacked Engelmann spruce in the vicinity of the AmeriFlux scaffold were sampled with constant heat sap flux sensors using the methodology of *Pataki et al.* [2000] and *Adelman et al.* [2008] which includes local sapwood allometrics to scale the measurement to the whole tree. Data were fit to a simple plant hydraulic model [*Oren et al.*, 1999] to relate m, the canopy conductance response to vapor pressure deficit (VPD), to $g_{s,\mathrm{ref}}$, the canopy conductance at a reference VPD of 1.0 kPa, and to test for differences between healthy and attacked trees (SAS PROC GLIMMIX, SAS Institute, Inc.). Calculation of m and $g_{s,\mathrm{ref}}$ followed *Ewers et al.* [2005]. In June, July, and August 2010, five healthy and five attacked trees in the vicinity of the scaffold were randomly selected and branches of from the upper third of the crown were collected using a shotgun. Samples were immediately rehydrated so that the measurements reflect photosynthetic capacity. Leaf CO_2 assimilation (A) and photosynthetic photon flux density (PPFD) were measured for each sample with an LI-6400 (Li-Cor, Inc., Lincoln, NE, USA) using the methodology of *Long and Bernacchi* [2003]. We used a logistic sigmoid (equation (1), with PPFD substituted for t and $t_{50} = 0$) to test for differences in light response curve parameters between healthy and attacked trees (SAS PROC NLMIXED, SAS Institute, Inc.).

2.3. GLEES AmeriFlux Data

All ecosystem flux measurements were made at GLEES AmeriFlux scaffold which was instrumented in October 2004. For summer daytime flux data, the 90% effective fetch of scaffold footprint extends 0.77 ± 0.18 km west at $266 \pm 58°$ (mean ± standard deviation) [*Gash*, 1986] which roughly overlaps the eastern half of the grid established for our dendrochronological survey (Figure S1) as well as the forest survey plots used by Speckman et al. (manuscript in preparation, 2014) to determine stand structure and the extent of beetle attacks and tree mortality. The scaffold is located in an area that is relatively flat for the region; along the average fetch, the slope runs ~4% downhill over 0.5 km to a streambed before rising upward at an ~6% grade. Though advective flows are possible with this topography [*Finnigan*, 2008], the unusually high turbulence at this site (average $u_* = 1$ m/s) is the greatest within the AmeriFlux network (http://ameriflux.ornl.gov/) and reduces flux uncertainty due to advection.

2.3.1. Meteorological Measurements

Ambient meteorological measurements were made of air temperature, T_a (RTD-810 resistance thermometer with OM5-1P4-N100-C signal conditioning module, Omega Engineering, Inc., Stamford, CT, USA, inside

076B-4 radiation shield, Met One Instruments, Inc., Grants Pass, OR, USA); relative humidity, RH (083D, Met One Instruments, Inc., also inside the 076B-4 radiation shield, except pre-August 2006 which was CS500, Campbell Scientific, Inc., Logan, UT, USA inside 41002 12-plate radiation shield, R. M. Young Company, Traverse City, MI, USA, mounted 28 m above the soil surface on another tower 80 m south); wind speed, U_a, and direction, α_a (05103-5 wind monitor, R. M. Young Company); pressure, p_a (AB-2AX Intellisensor II, Atmospheric Instrumentation Research, Inc., Boulder, CO, USA); CO_2 mole fraction mixing ratio, χ_c (LI-800, Li-Cor, Inc. until December 2008 then LI-7000, Li-Cor, Inc.); net radiation, R_n (Q*5.571 net radiometer, Radiation and Energy Balance Systems, Inc., Bellevue, WA); and upwelling and downwelling total PPFD (LI-190SA quantum sensor, Li-Cor Inc.), short-wave radiation, R_s (PSP, Eppley Laboratory, Newport, RI, USA), and long-wave radiation, R_l (PIR, Eppley Laboratory). All sensors were between 22.6 and 25.8 m above the soil surface. All were measured on a CR23X micrologger (Campbell Scientific, Inc.) at 0.5 or 1 Hz, were recorded every 5 min, had questionable values removed using the method of *Foken et al.* [2004], had small gaps linearly interpolated, were resampled to 30 min, and had gaps filled with surrogate or modeled data or a combination of both. All CO_2 sensors were monthly/periodically calibrated to reference tanks with at least 2% accuracy, though all references after May 2005 can be traced to AmeriFlux calibration standards with ±0.14 ppm accuracy. All other sensors were cleaned, calibrated, or exchanged as needed. Values were derived for dew point, T_d; vapor and saturation vapor pressures, p_v and $p_{v,\mathrm{sat}}$; VPD; vapor mole fraction mixing ratio, χ_v; air, dry air, vapor, and CO_2 densities, ρ_a, ρ_d, ρ_v, and ρ_c; and four-way net radiation, $R_{n,4\text{-way}}$. PPFD was separated into diffuse and direct components, $\mathrm{PPFD}_{\mathrm{diffuse}}$ and $\mathrm{PPFD}_{\mathrm{direct}}$ [*Campbell and Norman*, 1998; *Spitters et al.*, 1986].

2.3.2. Soil Measurements

Two vertical profiles of soil temperature, T_s, and volumetric water content, θ, were measured 90–100 m south of the scaffold in both a forest and meadow at 0.05, 0.10, 0.20, 0.51, and 1.02 m depths (Hydra probe, Vitel, Inc., Chantilly, VA). Two more profiles of T_s were measured ~1 m away from the meadow location and ~1.2 m away from each other at 0.03 and 0.09 m depths (24 AWG type-T thermocouple wire insulated with Omegabond 101, Omega Engineering, Inc.) and both accompanied with a soil heat-flux, G_s, measurement at 0.09 m (HFT-1, Radiation Energy Balance Systems, Inc.). Snow depth, z_{snow}, was measured with a depth sensor (Judd Communications, Salt Lake City, UT). Six measurements were averaged each half hour (CR10X micrologger, Campbell Scientific, Inc.) and questionable values were removed [*Foken et al.*, 2004]. Surface G_s was estimated by $G_{s,0} = G_{s,0.09} - C_s \partial T_s/\partial t \cdot z$ with the heat capacity of soil, C_s, a function of soil- and water-bulk density and specific heat capacity (estimated from θ and soil samples), depth, z, and time, t. Half-hourly profiles of T_s and θ were curve fit with a piecewise cubic Hermite to preserve the monotonicity between depths and integrated into shallow (0–10 cm) and deep (20–100 cm) soil temperature and moisture, $T_{s,\mathrm{shallow}}$, $T_{s,\mathrm{deep}}$, $\theta_{\mathrm{shallow}}$, and θ_{deep}. Surface G_s was gap filled (data were missing during summer 2006) using a model based on $R_{n,4\text{-way}}$ and T_s (specified by $G_s = aR_{n,4\text{-way}}{}^2 + bR_{n,4\text{-way}} + cT_s + d$, where $a = 0$ for $R_{n,4\text{-way}} < e$, function is piecewise continuous at e, and parameters a–e estimated with SAS PROC MODEL, SAS Institute, Inc.).

2.3.3. Eddy Covariance Measurements

Eddy covariance sensors were mounted on a 2 m boom extended due west and 22.65 m above the soil surface. Fast-response measurements of three-dimensional wind speed, u, v, and w; sonic virtual temperature, T_s (model SATI/3Vx sonic anemometer, Applied Technologies, Inc., Longmont, CO); ρ_v; and ρ_c (LI-7500 open-path infrared gas analyzer (IRGA), Li-Cor, Inc.) were recorded at 20 Hz on a data packer (model PAD-1202, Applied Technologies, Inc.) in serial connection to a CPU or a micrologger (CR3000, Campbell Scientific, Inc., beginning in January 2009). The IRGA was displaced 0.235 m east and 0.080 m south of the sonic anemometer. Beginning in January 2009, IRGA surface temperatures ($n = 3$) near the bottom and top windows and on one spar were measured (36 AWG type-T thermocouple wire insulated with Omegabond 101, Omega Engineering, Inc.) and recorded as half-hour averages. The canopy storage of CO_2 was measured with a vertical profile of χ_c sampled at 22.65, 19.3, 16.1, 12.9, 9.7, 6.5, 3.3, and 0.1 (adjusted with snowpack) m above the soil surface using a closed path IRGA (LI-6262, Li-Cor, Inc. until August 2008, then LI-7000, Li-Cor, Inc.).

Ecosystem fluxes were calculated using the eddy covariance technique [*Lee et al.*, 2004b]. Time series data were processed by half hour, despiked (using a modified version of *Højstrup* [1993] through 2008, then using a four-pass iterative median block filter (Text S1)), processed for quality assurance, quality control (QA/QC)

based on summary statistics (mean, standard deviation, skewness, kurtosis, and missing data [*Vickers and Mahrt*, 1997]), and IRGA calibration adjusted (for ρ_c based on periodic in situ reference gas calibrations, for ρ_v based on regression with the ambient meteorological ρ_v measurement [*Meek et al.*, 1998] (SAS PROC AUTOREG, SAS Institute, Inc.) and similar to *Loescher et al.* [2009] except on a longer time scale corresponding to weeks or months rather than half hours). Covariances among u, v, and w and with T_s, ρ_v, and ρ_c were calculated every half hour from the time series data, rotated into the long-term planar fit coordinate [*Lee et al.*, 2004a], and time-lag adjusted with the IRGA (half-hour time lags long-term modeled from wind speed and direction [*Horst and Lenschow*, 2009] with an offset optimized to maximize the absolute covariance within ±1 s lag). The covariances between w and u, T_s, ρ_v, and ρ_c were spectrally corrected (half-hour corrections [*Massman*, 2000; *Massman and Clement*, 2004] based on long-term modeled peak frequency [*Horst*, 1997] determined from median-pooled normalized cospectra). Sensible heat (H), water vapor (F_v), and CO_2 (F_c) ecosystem fluxes were calculated from the vertical wind covariances using the Webb-Pearman-Leuning (WPL) corrections [*Gu et al.*, 2012; *Massman and Lee*, 2002; *Webb et al.*, 1980] including the additional IRGA self-heating term [*Burba et al.*, 2008] (IRGA surface temperatures measured beginning in 2009, for preceding years modeled based on the 2009 measurements). The canopy storage of CO_2, $\overline{S}$ [*Lee and Massman*, 2011; W. J. Massman, unpublished derivation, 2010], was calculated using the piecewise cubic Hermite interpolated vertical profile of CO_2 measured within the canopy. The net ecosystem exchange of CO_2, NEE, was defined as $F_c + \overline{S}$ [*Lee and Massman*, 2011]. Evapotranspiration, ET, was defined as F_v and from which latent energy was derived. Atmospheric stability, z/L, and friction velocity, u_*, were derived from the eddy covariance data.

2.3.4. Canopy Conductance

Canopy conductance to CO_2 was calculated from the Penman-Monteith equation [*Monteith and Unsworth*, 2008] with aerodynamic and boundary layer resistance defined by *Massman et al.* [1994]. Potential evapotranspiration (PET) was calculated from the Penman-Monteith equation assuming infinite g_c [*Penman*, 1948].

2.4. Analysis

All analyses were conducted on daytime growing season data. We defined growing season as July–September, which corresponded closely (±8 days) to the intersection among all years of days without snow, standing water, or saturated shallow soil, with a strong daily NEE cycle, and before the magnitude of NEE rapidly decreases in the fall. Daytime was defined when PPFD $> 10\ \mu mol\ m^{-2}\ s^{-1}$. Data corresponding to $u_* < 0.2\ m\ s^{-1}$ (threshold determined using the method of *Gu et al.* [2005]) were not included. To limit outliers, g_c outside the range 0–300 $mmol\ m^{-2}\ s^{-1}$, PET outside the range −10 to 60 $mmol\ m^{-2}\ s^{-1}$, or gap-filled PPFD were not included. No flux data were gap filled. Daily average ET and NEE fluxes were determined by averaging across all non-missing day and night flux measurements with $u_* \geq 0.2\ m\ s^{-1}$ occurring at the same half hour of the day across the entire growing season.

We quantified the beetle epidemic impact on the ecosystem by testing for changes in the parameters describing the relationships between g_c, ET, PET, and NEE and each relative to their primary environmental drivers over time and by beetle phase. First, we used analysis of variance (ANOVA) to test for changes in g_c. Then, we tested ET relative to PET using a linear model with slope β_{PET} to detect mechanistic changes in g_c and ET [*Granier*, 1987]. This regression required correction for heteroscedasticity of errors (weight = $PET^{-0.7}$, determined a posteriori). With a change in conductance established, we determined the environmental drivers of g_c using linear model selection from a pool of candidate variables related to stomatal conductance: PPFD, T_a, VPD, $\theta_{shallow}$, θ_{deep}, χ_c, $T_{s,shallow}$, and $T_{s,deep}$ [*Delucia*, 1986; *Jarvis*, 1976; *Massman and Kaufmann*, 1991] where soil was separated into shallow (0–10 cm) and deep (20–100 cm) root zones and θ was a surrogate for leaf water potential assuming the possibility of anisohydric regulation, i.e., leaf water potential is not tightly controlled with increasing water stress, in spruce [*Ewers et al.*, 2005]. We then determined the environmental drivers of ET through linear model selection using candidate drivers from the Penman-Monteith equation: $R_{n,4\text{-way}} - G_s$ (diabatic term); VPD (adiabatic term); T_a, p_a, ρ_a, and ρ_v (variously related to the saturation vapor pressure, latent heat of vaporization, and psychrometric constant); U_a, u_*, and z/L (related to aerodynamic resistance), plus the identified drivers of g_c. Because Penman-Monteith is a semimechanistic model, only the relationships with g_c drivers were allowed to vary over time.

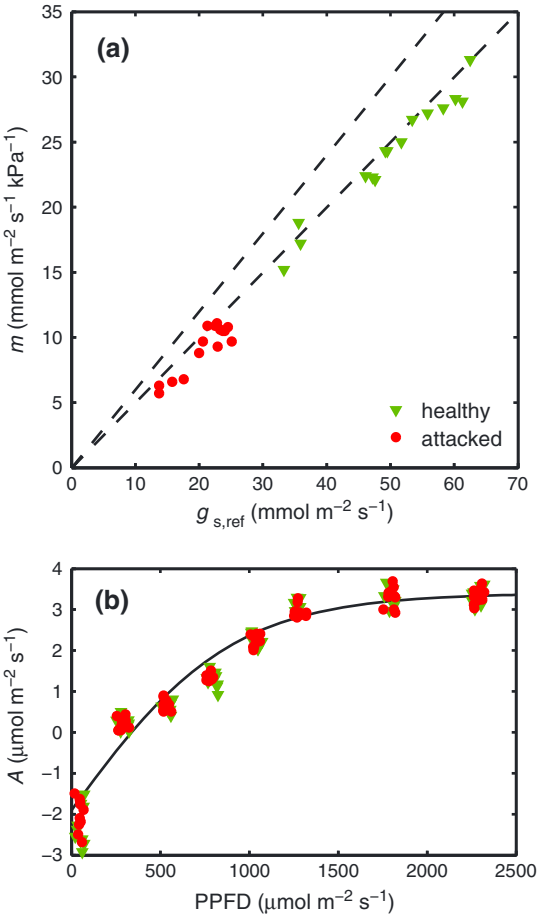

Figure 3. Tree physiological impacts of spruce beetle/blue-stain fungus on Engelmann spruce. (a) Sap flux data from healthy and attacked trees fit a simple hydraulic model [*Oren et al.*, 1999] relating the slope of the canopy conductance response to vapor pressure deficit VPD (m) to canopy conductance at a reference VPD of 1.0 kPa ($g_{s,ref}$). The region 0.5–0.6 (dashed lines) represents most plant taxa [*Katul et al.*, 2009]. (b) Photosynthetic assimilation (A) response to photosynthetic photon flux density (PPFD) from hydrated branches sampled from healthy and attacked trees fit to the logistic sigmoid function (equation (1)). Data are jittered 2% of full scale in Figure 3b for display purposes.

To qualitatively describe relationship between NEE and g_c, for each year, we fit a locally weighted regression (LOESS) curve [*Cleveland*, 1979; *Cleveland and Devlin*, 1988] which is a simple and flexible curve-fitting algorithm that gives a confidence limit on the predicted fit. We fit and compared the seven saturating response curves proposed by *Moffat* [2010] to have functional or historical (i.e., comparable to literature) significance for explaining the semiempirical NEE response to light (though we analogously extended these to a NEE response to g_c) plus a linear function and focused on the logistic sigmoid function (equation (2)) with β_{gc} (initial slope of the NEE versus g_c relationship) and A_{max} (maximum CO_2 assimilation rate).

$$\mathrm{NEE} = -A_{\max}\tanh\left(\frac{\beta_{g_c} g_c}{A_{\max}}\right) + \mathrm{Intercept} \quad (2)$$

To relate NEE to its environmental drivers, we fit three light response curves: a rectangular hyperbola (Michaelis-Menten, equation (3)), a logistic sigmoid [*Moffat*, 2010] (equation (4)), and a combination of diffuse and direct radiation (equation (5)) with A_{max} (maximum CO_2 assimilation rate), Φ, Φ_{direct}, and $\Phi_{diffuse}$ (quantum yields of photosynthesis for total, direct, and diffuse light), and R_d (day respiration). Each equation controlled for VPD [*Jarvis*, 1976] with a constant β_{VPD} (slope of the vapor deficit relationship):

$$\mathrm{NEE} = -\frac{A_{\max}\Phi\mathrm{PPFD}}{A_{\max} + \Phi\mathrm{PPFD}}(1 - \beta_{\mathrm{VPD}}\mathrm{VPD}) + R_d \quad (3)$$

$$\mathrm{NEE} = -A_{\max}\tanh\left(\frac{\Phi\mathrm{PPFD}}{A_{\max}}\right)(1 - \beta_{\mathrm{VPD}}\mathrm{VPD}) + R_d \quad (4)$$

$$\mathrm{NEE} = -(\Phi_{\mathrm{direct}}\mathrm{PPFD}_{\mathrm{direct}} + \Phi_{\mathrm{diffuse}}\mathrm{PPFD}_{\mathrm{diffuse}})(1 - \beta_{\mathrm{VPD}}\mathrm{VPD}) + R_d \quad (5)$$

Model selection was limited to variables improving overall R^2 by at least 0.05 (SAS PROC GLMSELECT, SAS Institute, Inc.). All analyses were done while testing and correcting for autocorrelation of errors (SAS PROC MODEL, SAS Institute, Inc., one time lag) [*Bender and Heinemann*, 1995; *Meek et al.*, 1998]. Parameters were compared by year and by epidemic phase, except β_{VPD} which was held constant. All comparisons were Bonferroni corrected for multiple comparisons [*Hochberg and Tamhane*, 1987]. We checked the sensitivity of all analyses to the Penman-Monteith calculation using other definitions of aerodynamic resistance [*Brutsaert*, 1982; *Campbell and Norman*, 1998; *Monteith and Unsworth*, 2008; *Thom and Oliver*, 1977] as well as the definition of the growing season.

We conducted a meta-analysis of our results to reconcile changes in parameters that most represent the diminishment in ET and NEE, while relating these changes to ecosystem structure and loss of overstory flux. Declines during epidemic I were not used to determine changes in ecosystem structure because the interpretation of these years depends on selection of hypothesis a or b. Simultaneously, we tested the sensitivity

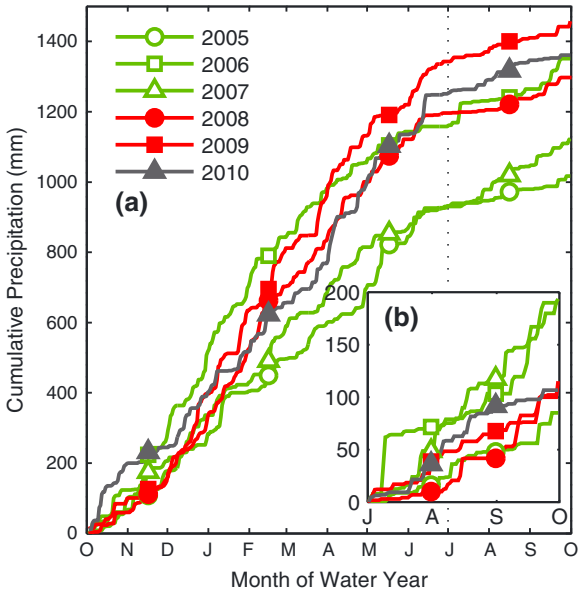

Figure 4. Cumulative precipitation at GLEES during (a) the water year (1 October to 30 September) and (b) the summer growing season (July–September) for the endemic (2005–2007) and epidemic (2008–2010) years. Data from the National Atmospheric Deposition Program WY95 site (http://nadp.sws.uiuc.edu/) 200 m from the AmeriFlux scaffold.

of β_{PET} to the formulation of boundary layer resistance [*Brutsaert*, 1982; *Kaimal and Finnigan*, 1994; *Massman et al.*, 1994; *Monteith and Unsworth*, 2008; *Thom and Oliver*, 1977]. This was done using a hierarchical Bayesian random-effects model [*Gelman et al.*, 2004; *Rubin*, 1981]. The modeled data were the mean and standard errors of the regression parameters Φ, A_{max}, Φ_{direct}, $\Phi_{diffuse}$, and β_{PET}. Gamma distributions were used as priors for parameters representing the distributions of the regression parameters during the endemic phase. Priors for the hyperparameters were either flat distributions (pre-epidemic contribution of transpiration, *T*, to ET and overstory to total ecosystem flux) or gamma distributions (the relative changes in overstory, NEE, and ET from the endemic to epidemic I or II phases; random effects in the changes in NEE and ET due to choice of boundary layer resistance or light response parameter). Analysis was conducted with OpenBUGS (version 3.2.2 rev 1063, Members of OpenBUGS Project Management Group). The source code is provided in Text S2.

3. Results

3.1. When Trees Were Attacked and When They Died

We successfully cored and dated 109 Engelmann spruce and 38 subalpine fir trees, of which 79 were recently dead including 74 spruce (Figure 1 and Table S1). Spruce were older and larger (268 ± 163 years mean ± standard deviation, 44 ± 23 cm diameter at breast height) than fir (161 ± 76 years, 27 ± 11 cm) while dead spruce were older and larger (307 ± 165 years, 53 ± 23 cm) than live spruce (186 ± 126 years and 25 ± 9 cm) (Table S1). The average age to coring height was 35 ± 17 years. Tree establishment dated to the 1200s while the age structure coincided with climatic events and not disturbances (Text S3).

The number of attacks was greatest in 2008 (Figure 1). The regression parameters (estimate ± standard error) for the logistic sigmoid predicting attacks were $y_{50} = 0.30 \pm 0.004\%$, $\Delta_y = 0.30 \pm 0.007\%$, $m = 0.00037 \pm 0.000016\%$/d, $t_{50} =$ 3 March 2008 ± 0.0 day (Figure 1). The reduction in LAI following mortality occurred much later (1.8 ± 0.9 years); the regression parameters for LAI were $y_{50} = 3.76 \pm 0.198\ m^2\ m^{-2}$, $\Delta_y = 0.89 \pm 0.203\ m^2\ m^{-2}$, $m = -0.00107 \pm 0.000315\ m^2\ m^{-2}$/d, $t_{50} =$ 3 January 2010 ± 339 days (Figure 1).

3.2. The Physiology Effect of Beetle Attacks on Spruce Trees

Our sap flux data show that the conductance $g_{s,ref}$ was significantly lower for Engelmann spruce attacked by spruce beetle/blue-stain fungus ($p < 0.0001$) but that the slope of the relationship *m* to $g_{s,ref}$ was not different for healthy or attacked trees ($p = 0.81$) or the 0.5–0.6 region ($p > 0.61$) described by *Katul et al.* [2009] (Figure 3a). There also was no difference in photosynthesis between hydrated branches sampled from healthy or attacked trees ($p > 0.18$ for all parameters after fitting the logistic sigmoid function (equation (1)); Figure 3b).

3.3. Precipitation and Soil Moisture

The climate at GLEES is dominated by winter moisture (Figure 4a). More precipitation accumulated from the beginning of the water year (1 October) until the end of June during the epidemic years, while the accumulations in 2005 and 2007 were noticeably deficient by over 200 mm (Figure 4a). Summer precipitation at GLEES is much lower, and though 2006 and 2007 were relatively moist, 2005 was 30 mm drier than any other year (Figure 4b). Soil moisture was generally equal or higher during the epidemic years: $\theta_{shallow}$ was

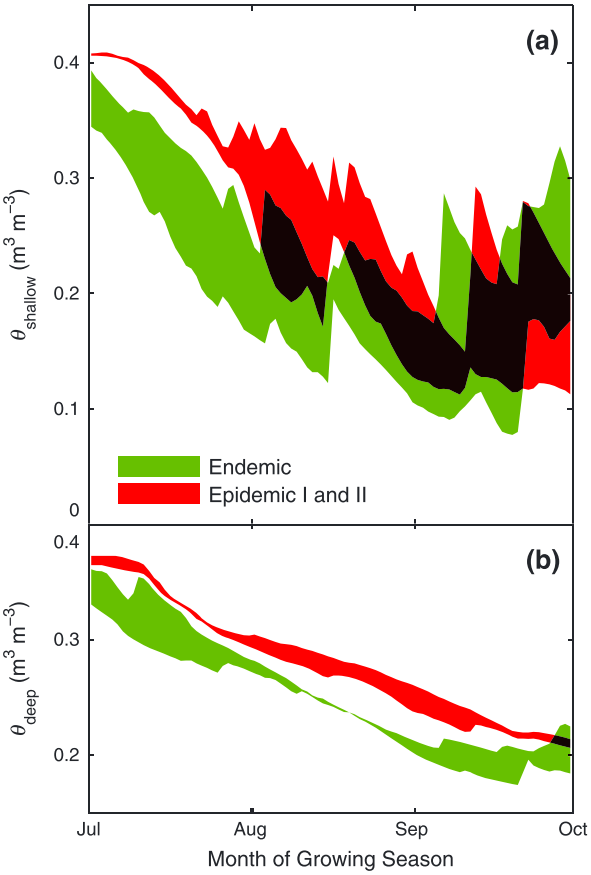

Figure 5. Range of daily (a) shallow and (b) deep soil moisture (θ) during the summer growing season (July–September) for the endemic (2005–2007) and epidemic (2008–2010) years.

higher in July before becoming more similar to endemic levels during middle and late summer (Figure 5a) and θ_{deep} was higher throughout the entire season (Figure 5b).

3.4. Average Daily Ecosystem Fluxes

The average daily ET fluxes appeared higher during the endemic years (Figure 6a) and when extrapolated over the entire growing season ranged from 245 to 260 mm during 2005–2007 and 204 to 218 mm during the epidemic years 2008–2010. The average daily NEE fluxes appeared to decrease in magnitude during epidemic I and then further in epidemic II (Figure 6b). When extrapolated over the growing season, the ecosystem carbon sink ranged from 163 to 234 g C m^{-2} for the endemic years, 83 to 112 g C m^{-2} for epidemic I, and -5 g C m^{-2} for epidemic II.

Yet these observations are difficult to test and support statistically; thus, we focus our analysis on response curves of half hourly fluxes in the following sections. For these, all parameter comparisons were significant ($p < 0.05$) unless otherwise noted. All analyses included an autoregressive model (Durbin-Watson statistic increased from 0.55–1.26 to 1.98–2.27) that typically increased the relative standard errors of parameters but, in some circumstances, altered the parameter estimates (-7% for Φ, -10% for A_{max}, -17% for R_d, -19% for Φ_{direct}, $+22\%$ for $\Phi_{diffuse}$, and -65% for β_{gc}). The Breusch-Pagan test for heteroscedasticity of errors in the ET versus PET relationship was significant ($p < 0.0001$) before controlling with a weighted regression ($p = 0.08$).

3.5. Changes in Canopy Conductance and Evapotranspiration

During the spruce beetle epidemic, average g_c decreased 17% while ET decreased 22% relative to PET (Tables 1 and 2, and Figures S2a–S2c versus S2d–S2f). There were no differences in g_c between any of the endemic years (2005–2007) nor were there differences between any of the epidemic years (phases I and II, 2008–2010) except for some minor intercept differences (<0.2 mmol m^{-2} s^{-1}) in the ET versus PET relationship (Tables 1 and 2). The ET/PET analyses were sensitive to the definition of aerodynamic resistance; there were significant differences between epidemic I and II and greater parameter decreases (Tables S2 and S3).

Through model selection, PPFD was identified as the primary environmental driver of g_c ($R^2 = 0.21$), followed by VPD ($R^2 = 0.39$ for two drivers), and $T_{s,shallow}$ ($R^2 = 0.47$ for three drivers). No other driver (T_a, $T_{s,deep}$, $\theta_{shallow}$, θ_{deep}, or χ_c) increased R^2 by more than 0.01 and the maximum R^2 with all drivers was 0.50. Model selection was also performed without each driver to determine its uniqueness: Without PPFD then VPD was selected ($R^2 = 0.10$), without VPD then T_a was selected ($R^2 = 0.28$ for two drivers), and without $T_{s,shallow}$ then T_a was selected ($R^2 = 0.44$ for three drivers). The g_c response to PPFD did change between years (highest in 2007 and lowest in 2008 and 2009) and it significantly decreased 14% in epidemic I while the 9% decrease in epidemic II was not significant (Tables 1 and 2). The g_c response to VPD did not change over time. Tree hydraulic analysis of sap flux data supported hydraulic failure as the mechanism for g_c decline (Figure 3a). The g_c response to $T_{s,shallow}$ also changed between years (highest in 2005, lowest in 2007–2010) which equaled a 20% decrease during epidemic I and a 24% in epidemic II (Tables 1 and 2).

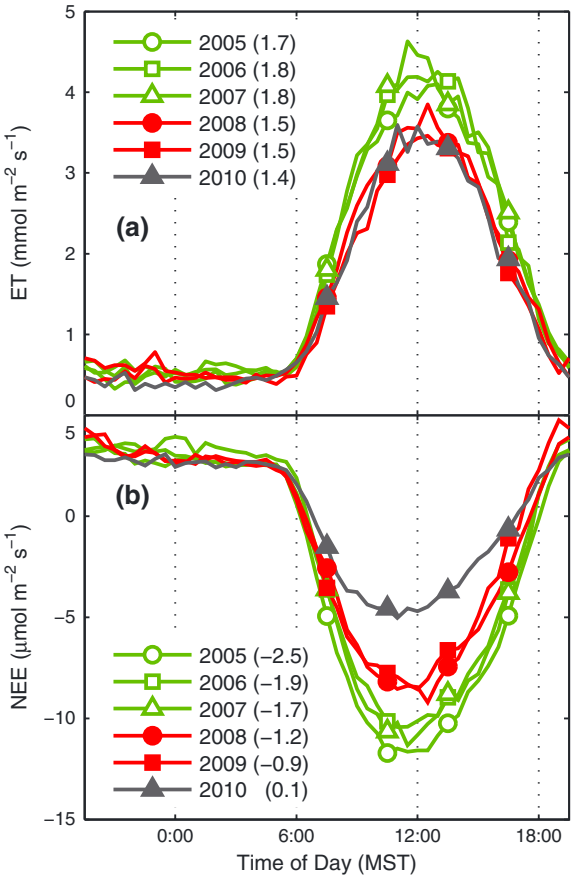

Figure 6. Average (a) evapotranspiration (ET) and (b) net ecosystem exchange of CO_2 (NEE) fluxes during the summer growing season (July–September) for the endemic (2005–2007) and epidemic (2008–2010) years. Total daily averages are in parentheses.

PPFD was the primary environmental driver of ET ($R^2 = 0.59$) followed only by $T_{s,\text{shallow}}$ ($R^2 = 0.66$ for two drivers). No other driver increased R^2 more than 0.01 and the maximum R^2 with all drivers was 0.69. We similarly evaluated uniqueness; without PPFD then $R_{n,4\text{-way}} - G$ was selected ($R^2 = 0.57$) and without $T_{s,\text{shallow}}$ then ρ_a was selected ($R^2 = 0.63$ for two drivers). The ET response to PPFD varied between years (highest in 2006–2007 and lowest in 2005 and 2008–2010) and decreased 17% in epidemic I and 19% in epidemic II (Tables 1 and 2, and Figures 7a–7c versus 7d–7f). The ET response to $T_{s,\text{shallow}}$ also changed between years (highest in 2005 and lowest in 2008) and decreased 13% in epidemic I and 12% in epidemic II (Tables 1 and 2).

3.6. Changes in NEE

Compared to the LOESS fit, the NEE response to g_c followed saturation curves similar to those proposed by *Moffat* [2010] (Figure 8). Of those, we chose to fit and test the logistic sigmoid (equation (2) and Figure 8) because it had high R^2 (highest among the three-parameter models), consistent convergence, and low standard errors for parameter estimates (comparison data not shown) with no difference in residual patterns. We focused only on the β_{gc} parameter relating the slope of the NEE versus g_c relationship, which did not change in epidemic I or between any year during 2005–2009 but decreased 46% in epidemic II (Tables 1 and 2, and Figures 8a–8e versus 8f). The lack of change in this relationship before epidemic II is supported by the lack of change in the response of needle photosynthesis to PPFD as the trees died (Figure 3b). Thus, hydraulic failure led to low g_c as water transport failed, but the trees were able to maintain leaf water status such that photosynthetic biochemistry did not decline.

The NEE response to light was best fit with the diffuse-direct model (equation (5), $R^2 = 0.74$) than either the Michaelis-Menten (equation (3)) or logistic sigmoid models (equation (4) and Figure 9) ($R^2 = 0.66$ for both) with no difference in residual patterns. When compared to Michaelis-Menten, the logistic sigmoid parameter estimates were smaller (−12% for R_d, −30% for Φ, and −40% for A_{max}) with smaller relative standard errors (−38% for Φ and −40% for A_{max}; Tables 1 and 2). For all models, inclusion of the VPD term increased the R^2 by 0.04.

In general, there were no differences detected in R_d between beetle phases, except a 0.5 μmol m^{-2} s^{-1} increase in epidemic I with the diffuse-direct model (Table 2). R_d did vary slightly by year with the logistic sigmoid and diffuse-direct models: R_d was highest in 2009 and lowest in 2006 (along with 2005 and 2010 with diffuse-direct) with a maximum difference of 1.0 μmol m^{-2} s^{-1} (Table 1). Φ, Φ_{direct}, and Φ_{diffuse} all decreased in epidemic I (−24% to −31% for Φ, −8% for Φ_{direct}, and −19% for Φ_{diffuse}; Table 2 and Figures 9a–9c versus 9d and 9e) and then decreased further in epidemic II (−50% to −52% for Φ, −56% for Φ_{direct}, and −41% for Φ_{diffuse}; Table 2 and Figures 9a–9c versus 9f). These trends generally occurred between years with a few exceptions when there were no statistical differences: Φ between 2006 and 2008 (Michaelis-Menten), 2009 and 2010 (Michaelis-Menten), and 2006 and 2008–2009 (logistic sigmoid); Φ_{direct} between 2005–2007 and

Table 1. Summary of All Statistical Tests With Respect to Year

			Year		
Comparison	Function	Regression Parameters	2005	2006	2007
g_c	ANOVA	g_c (mmol m^{-2} s^{-1})	115.9 (2.27)^{b}	124.2 (2.47)^{b}	116.6 (2.65)^{b}
		φ	−0.668 (0.0085)*		
ET versus PET	Linear	Intercept (mmol m^{-2} s^{-1})	0.476 (0.0351)^{a,b}	0.517 (0.0356)^{b}	0.529 (0.0423)^{b}
		β_{PET} (mmol mmol^{-1})	0.0907 (0.00204)^{b}	0.0994 (0.00215)^{b}	0.0976 (0.00245)^{b}
		φ	−0.594 (0.0087)*		
g_c versus environmental drivers	Linear	Intercept (mmol m^{-2} s^{-1})	81.9 (2.14)*		
		β_{PPFD} (mmol μmol^{-1})	0.0519 (0.00210)^{a,b}	0.0603 (0.00229)^{b,c}	0.0619 (0.00257)^{c}
		β_{VPD} (mmol m^{-2} s^{-1} kPa^{-1})	−102.5 (4.22)^{a}	−89.3 (4.56)^{a}	−89.4 (4.94)^{a}
		$\beta_{Ts,shallow}$ (mmol m^{-2} s^{-1} C^{-1})	8.80 (0.472)^{b}	7.30 (0.461)^{a,b}	6.53 (0.516)^{a}
		φ	−0.403 (0.0101)*		
ET versus environmental drivers	Linear	Intercept (mmol m^{-2} s^{-1})	−0.58 (0.049)*		
		β_{PPFD} (mmol μmol^{-1})	0.00187 (0.000046)^{a}	0.00214 (0.000048)^{b}	0.00231 (0.000053)^{b}
		$\beta_{Ts,shallow}$ (mmol m^{-2} s^{-1} C^{-1})	0.162 (0.0073)^{c}	0.157 (0.0070)^{b,c}	0.134 (0.0076)^{a,b}
		φ	−0.478 (0.0087)*		
NEE versus g_c	Logistic sigmoid (equation (1))	Intercept (μmol m^{-2} s^{-1})	0.2 (0.30)^{a}	0.9 (0.31)^{a,b}	1.0 (0.32)^{a,b}
		$\beta_{gc,C}$ (μmol mmol^{-1})	0.0463 (0.00400)^{b}	0.0392 (0.00350)^{b}	0.0427 (0.00344)^{b}
		A_{max} (μmol m^{-2} s^{-1})	9.3 (0.52)^{a,b}	10.0 (0.82)^{b}	13.3 (1.73)^{b}
		φ	−0.893 (0.0057)*		
NEE versus environmental drivers	Rectangular hyperbola (Michaelis-Menten, equation (2))	R_d (μmol m^{-2} s^{-1})	2.8 (0.21)^{a}	2.6 (0.22)^{a}	3.4 (0.24)^{a}
		Φ (mol mol^{-1})	0.0281 (0.00156)^{d}	0.0225 (0.00143)^{c,d}	0.0242 (0.00147)^{d}
		A_{max} (μmol m^{-2} s^{-1})	27.1 (0.98)^{b,c}	26.8 (1.19)^{b,c}	31.3 (1.49)^{c,d}
		β_{VPD} (kPa^{-1})	0.202 (0.0098)*		
		φ	−0.773 (0.0065)*		
	Logistic sigmoid (equation (3))	R_d (μmol m^{-2} s^{-1})	2.4 (0.19)^{a,b}	2.2 (0.20)^{a}	3.0 (0.21)^{a,b}
		Φ (mol mol^{-1})	0.0183 (0.00064)^{d}	0.0153 (0.00060)^{b,c}	0.0165 (0.00062)^{d,c}
		A_{max} (μmol m^{-2} s^{-1})	17.3 (0.43)^{c,d}	16.4 (0.45)^{c}	18.7 (0.55)^{d}
		β_{VPD} (kPa^{-1})	0.200 (0.0102)*		
		φ	−0.775 (0.0065)*		
	Linear (equation (4))	R_d (μmol m^{-2} s^{-1})	2.6 (0.17)^{a}	2.6 (0.18)^{a}	3.3 (0.20)^{a,b}
		Φ_{direct} (mol mol^{-1})	0.0076 (0.00020)^{c}	0.0072 (0.00020)^{c}	0.0084 (0.00023)^{d}
		$\Phi_{diffuse}$ (mol mol^{-1})	0.0205 (0.00050)^{e}	0.0176 (0.00049)^{c,d}	0.0192 (0.00054)^{d,e}
		β_{VPD} (kPa^{-1})	0.223 (0.0080)*		
		φ	−0.712 (0.0072)*		

2009; and $\Phi_{diffuse}$ between 2006 and 2009 (Table 1). A_{max} did not change until epidemic II when it decreased 51% (Table 2 and Figures 9a–9e versus 9f). There was some variation from 2005 to 2009: A_{max} was highest in 2009 (plus 2007 with the logistic sigmoid) and lowest in 2008.

3.7. Meta-analysis

Posterior densities for the decreases in ET and NEE were approximately normally distributed. ET changed by −28 ± 4% and −36 ± 4% during epidemic I and II (the 95% credible intervals overlapped), while NEE changed by −13 ± 6% and −51 ± 3% similarly (mean ± standard deviation; Table S4). The pre-epidemic contribution of overstory to total ecosystem flux as well as the loss of overstory flux was >50% (Figures S3a and S3b, and Table S4) and highly correlated (Figure S3d). While the contribution of *T* to ET had a large range (95% credible interval from 55 to 89%; Table S4), the posterior density was more defined with an obvious peak at 71% (Figure S3c).

4. Discussion

We observed through cessation of tree ring growth [*Mast and Veblen*, 1994] that even though beetle attacks occurred throughout the past decade, 2008 was the year both of peak attack and when the number of impacted trees crossed the 50% threshold (Figure 1). But, as observed in the MODIS LAI data (Figure 1) and our repeat photos (Figure 2), observable tree mortality had a different temporal pattern from attacks, and did not occur until 1.8 ± 0.9 years later. This supports our definition of three phases (endemic, epidemic I, and epidemic II), is consistent with previous observations in Engelmann

Table 1. (continued)

Year				Without Correcting for Autocorrelation of Errors			Correcting for Autocorrelation of Errors		
2008	2009	2010	*N*	R^2	RMSE	DW	R^2	RMSE	DW
96.5 (2.43)[a]	96.4 (2.47)[a]	101.1 (2.37)[a]	10398	0.039	55.7	0.70	0.397	44.1	2.07
0.482 (0.0382)[a,b] 0.0725 (0.00219)[a]	0.362 (0.0374)[a] 0.0795 (0.00237)[a]	0.393 (0.0419)[a,b] 0.0735 (0.00226)[a]	10142	0.518	1.06	0.81	0.756	0.29	2.10
0.0495 (0.00225)[a] −89.3 (4.68)[a] 6.13 (0.522)[a]	0.0494 (0.00221)[a] −93.8 (4.42)[a] 6.10 (0.503)[a]	0.0523 (0.00215)[a,b,c] −94.8 (4.02)[a] 5.84 (0.464)[a]	10396	0.473	41.3	1.26	0.542	38.5	2.03
0.00180 (0.000048)[a] 0.129 (0.0078)[a]	0.00168 (0.000048)[a] 0.136 (0.0079)[a,b]	0.00168 (0.000047)[a] 0.133 (0.0080)[a,b]	11338	0.658	0.97	1.09	0.729	0.86	2.16
1.4 (0.29)[b] 0.0383 (0.00425)[b] 7.0 (0.53)[a]	1.2 (0.28)[a,b] 0.0393 (0.00364)[b] 8.4 (0.71)[a,b]	1.2 (0.27)[a,b] 0.0227 (0.00312)[a] 6.5 (1.37)[a,b]	10387	0.463	3.7	0.66	0.760	2.4	1.98
2.9 (0.22)[a] 0.0178 (0.00133)[b,c] 24.6 (1.47)[b]	3.4 (0.21)[a] 0.0170 (0.00104)[a,b] 35.5 (2.36)[d]	2.5 (0.21)[a] 0.0120 (0.00144)[a] 13.8 (1.13)[a]	11327	0.665	3.0	0.56	0.846	2.0	2.25
2.6 (0.20)[a,b] 0.0127 (0.00060)[b] 14.4 (0.50)[b]	3.1 (0.19)[b] 0.0132 (0.00051)[b] 18.7 (0.64)[d]	2.4 (0.20)[a,b] 0.0085 (0.00062)[a] 8.5 (0.40)[a]	11327	0.661	3.0	0.55	0.846	2.0	2.25
2.9 (0.18)[a,b] 0.0063 (0.00021)[b] 0.0154 (0.00051)[b]	3.6 (0.18)[b] 0.0077 (0.00020)[c,d] 0.0156 (0.00048)[b,c]	2.8 (0.18)[a] 0.0034 (0.00019)[a] 0.0112 (0.00050)[a]	11327	0.749	2.6	0.78	0.856	2.0	2.27

Relating canopy conductance (g_c), evapotranspiration (ET), potential evapotranspiration (PET), and net ecosystem exchange of CO_2 (NEE) to each other and to environmental drivers: total, direct, and diffuse photosynthetic photon flux density (PPFD, $PPFD_{direct}$, and $PPFD_{diffuse}$), vapor pressure deficit (VPD), and shallow soil temperature ($T_{s,shallow}$). Tests were between parameters: regression intercepts and slopes (β), maximum CO_2 assimilation rate (A_{max}), quantum yields of photosynthesis for total, direct, and diffuse light (Φ, Φ_{direct}, and $\Phi_{diffuse}$), and day respiration (R_d). Standard errors are in parenthesis. Statistically different parameters ($p < 0.05$) in each row are designated with different letter superscripts (a-e). All parameters estimated while controlling for autocorrelation of errors (autoregression coefficient (φ) and Durbin-Watson statistic (DW)). The ET versus PET analysis also controlled for heteroscedasticity of errors (Breusch-Pagan test $p = 0.0814$).
*These values were fixed over time.

spruce of a 1 to 3 year delay between attack and mortality [*Mast and Veblen*, 1994], is explained by our tree physiology data that show attacked trees still maintain leaf biochemistry, and supports hypothesis b and its predictions.

The first-order effects of a beetle epidemic occur at the plant scale. Blue-stain fungi impacts on the hydraulics of Engelmann spruce fit the expectations of a simple plant hydraulic model [*Oren et al.*, 1999] (Figure 3a). Because the slopes of healthy and attacked trees are not different from each other or the 0.5–0.6 region [*Katul et al.*, 2009] (Figure 3a), this indicates that the trees are regulating minimum leaf water potential as hydraulic conductance declines [*Ewers et al.*, 2005; *Oren et al.*, 1999]. At the same time, the blue-stain fungi do not impact leaf photosynthetic biochemistry (Figure 3b) but hydraulic limitation leads to decreased C uptake from gas exchange limitations while trees are dying from attacks. These data strongly support the hypothesis that trees are dying from hydraulic failure by fungal xylem occlusion but maintain leaf biochemistry by reducing stomatal conductance to prevent excessive dehydration of foliage.

To evaluate our two competing hypothesis that (a) changes in ecosystem fluxes can be inferred simply from the observable patterns of mortality or (b) that physiological impacts in the attacked trees must also be incorporated, we must understand how the responses of g_c, ET, and NEE to their environmental drivers

Journal of Geophysical Research: Biogeosciences 10.1002/2013JG002597

Table 2. Summary of All Statistical Tests With Respect to Beetle Phase

			Beetle Phase				Without Correcting for Autocorrelation of Errors			Correcting for Autocorrelation of Errors		
Comparison	Function	Regression Parameters	Endemic	Epidemic I	Epidemic II	N	R^2	RMSE	DW	R^2	RMSE	DW
g_c	ANOVA	g_c (mmol m^{-2} s^{-1})	118.8 (1.42)^b	96.5 (1.74)^a	101.2 (2.38)^a	10398	0.036	55.8	0.70	0.397	44.1	2.08
		φ	−0.670 (0.0085)*									
ET versus PET	Linear	Intercept (mmol m^{-2} s^{-1})	0.505 (0.0216)^a	0.423 (0.0268)^a	0.395 (0.0420)^a	10142	0.512	1.06	0.80	0.755	0.29	2.10
		β_{PET} (mmol mmol^{-1})	0.0953 (0.00128)^b	0.0756 (0.00162)^a	0.0734 (0.00227)^a							
		φ	−0.598 (0.0086)*									
g_c versus environmental drivers	Linear	Intercept (mmol m^{-2} s^{-1})	81.8 (2.15)*			10396	0.468	41.4	1.25	0.540	38.5	2.03
		β_{PPFD} (mmol μmol^{-1})	0.0575 (0.00135)^b	0.0494 (0.00159)^a	0.0523 (0.00216)^{a,b}							
		β_{VPD} (mmol m^{-2} s^{-1} kPa^{-1})	−94.4 (2.64)^a	−91.2 (3.24)^a	−94.8 (4.06)^a							
		$\beta_{Ts,shallow}$ (mmol m^{-2} s^{-1} C^{-1})	7.65 (0.315)^b	6.10 (0.388)^a	5.85 (0.467)^a							
		φ	−0.409 (0.0101)*									
ET versus environmental drivers	Linear	Intercept (mmol m^{-2} s^{-1})	−0.58 (0.049)*			11338	0.654	0.97	1.08	0.728	0.86	2.17
		β_{PPFD} (mmol μmol^{-1})	0.00208 (0.000029)^b	0.00174 (0.000035)^a	0.00168 (0.000048)^a							
		$\beta_{Ts,shallow}$ (mmol m^{-2} s^{-1} C^{-1})	0.152 (0.0056)^b	0.132 (0.0066)^a	0.133 (0.0081)^a							
		φ	−0.483 (0.0087)*									
NEE versus g_c	Logistic sigmoid (equation (4))	Intercept (μmol m^{-2} s^{-1})	0.6 (0.18)^a	1.3 (0.20)^b	1.2 (0.27)^{a,b}	10387	0.458	3.7	0.65	0.759	2.5	1.98
		$\beta_{gc,C}$ (μmol mmol^{-1})	0.0423 (0.00210)^b	0.0389 (0.00279)^b	0.0227 (0.00313)^a							
		A_{max} (μmol m^{-2} s^{-1})	10.4 (0.48)^b	7.6 (0.43)^a	6.5 (1.37)^{ab}							
		φ	−0.893 (0.0057)*									
NEE versus environmental drivers	Rectangular hyperbola (Michaelis-Menten, equation (1)	R_d (μmol m^{-2} s^{-1})	2.9 (0.13)^a	3.1 (0.15)^a	2.5 (0.21)^a	11327	0.659	3.0	0.54	0.845	2.0	2.25
		Φ (mol mol^{-1})	0.0251 (0.00087)^c	0.0172 (0.00082)^b	0.0120 (0.00145)^a							
		A_{max} (μmol m^{-2} s^{-1})	27.9 (0.77)^b	29.8 (1.40)^b	13.8 (1.12)^a							
		β_{VPD} (kPa^{-1})	0.199 (0.0099)*									
		φ	−0.773 (0.0065)*									
	Logistic sigmoid (equation (2))	R_d (μmol m^{-2} s^{-1})	2.5 (0.12)^a	2.8 (0.14)^a	2.4 (0.20)^a	11327	0.655	3.1	0.54	0.845	2.0	2.25
		Φ (mol mol^{-1})	0.0167 (0.00038)^c	0.0128 (0.00039)^b	0.0084 (0.00062)^a							
		A_{max} (μmol m^{-2} s^{-1})	17.3 (0.33)^b	16.5 (0.44)^b	8.5 (0.40)^a							
		β_{VPD} (kPa^{-1})	0.197 (0.0103)*									
		φ	−0.776 (0.0065)*									
	Linear (equation (3))	R_d (μmol m^{-2} s^{-1})	2.8 (0.11)^a	3.3 (0.13)^b	2.8 (0.18)^{a,b}	11327	0.740	2.6	0.75	0.855	2.0	2.28
		Φ_{direct} (mol mol^{-1})	0.0076 (0.00014)^c	0.0070 (0.00016)^b	0.0033 (0.00019)^a							
		$\Phi_{diffuse}$ (mol mol^{-1})	0.0190 (0.00032)^c	0.0154 (0.00036)^b	0.0111 (0.00050)^a							
		β_{VPD} (kPa^{-1})	0.219 (0.0081)*									
		φ	−0.718 (0.0072)*									

Relating canopy conductance (g_c), evapotranspiration (ET), potential evapotranspiration (PET), and net ecosystem exchange of CO_2 (NEE) to each other and to environmental drivers: total, direct, and diffuse photosynthetic photon flux density (PPFD, $PPFD_{direct}$, and $PPFD_{diffuse}$), vapor pressure deficit (VPD), and shallow soil temperature ($T_{s,shallow}$). Tests were between parameters: regression intercepts and slopes (β), maximum CO_2 assimilation rate (A_{max}), quantum yields of photosynthesis for total, direct, and diffuse light (Φ, Φ_{direct}, and $\Phi_{diffuse}$), and day respiration (R_d). Standard errors are in parenthesis. Statistically different parameters ($p < 0.05$) in each row are designated with different letter superscripts (a-c). All parameters estimated while controlling for autocorrelation of errors (autoregression coefficient (φ) and Durbin-Watson statistic (DW)). The ET versus PET analysis also controlled for heteroscedasticity of errors (Breusch-Pagan test $p = 0.0728$).

*These values were fixed over time.

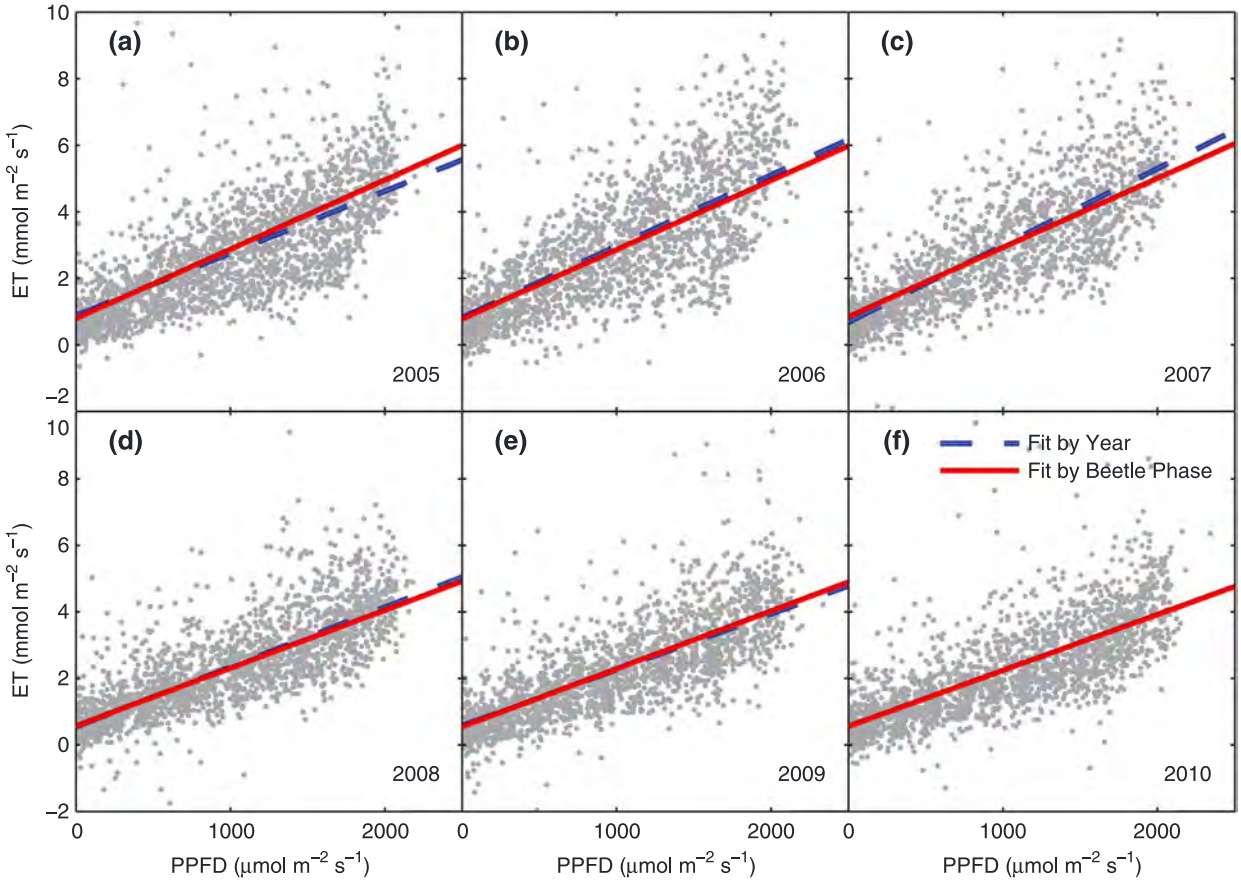

Figure 7. Evapotranspiration (ET) response to photosynthetic photon flux density (PPFD) for daytime growing season modeled by year and for the three phases of the beetle outbreak: (a–c) endemic, (d and e) epidemic I, and (f) epidemic II. Model parameters are in Tables 1 and 2. The response to average soil temperature ($T_{s,shallow}$) was included as a constant.

changed over the course of the beetle outbreak. That is, which explains the data better: (a) g_c, ET, and NEE all diminish in concert with mortality and reduced LAI, or (b) there was an initial phase (epidemic I) corresponding to beetle attacks and dominated by hydraulic failure (reduced g_c and ET) and restricted gas exchange (reduced NEE) followed by a second phase (epidemic II) corresponding to mortality (further reduced NEE).

4.1. Changes in Canopy Conductance and Evapotranspiration

The bark beetles fundamentally altered the conductance of water vapor from the ecosystem during the first phase of the epidemic. There was a 22% decreased in ET relative to PET that occurred before the 2008 summer growing season (Tables 1 and 2, and Figure S2). Because the ET versus PET relationship implicitly accounts for climate through the Penman-Monteith equation, this reduction reflects a mechanistic change in the ecosystem independent of any changes in the environment. We propose that xylem occlusion caused by the beetle-associated blue-stain fungi is the cause of this mechanistic change.

Blue-stain fungi play a vital role in bark beetle infestations by helping overcome tree defenses with fungal penetration and sapwood occlusion [*Paine et al.*, 1997] and can do so quickly over a few weeks as observed with mountain pine beetle [*Hubbard et al.*, 2013; *Yamaoka et al.*, 1990]. *Leptographium abietinum* is the most common mycelial fungus isolated from spruce beetle [*Six and Bentz*, 2003] though *Ceratocystis rufipenni* is often found in infested Engelmann spruce [*Wingfield et al.*, 1997]. *C. rufipenni* is believed to be more important in helping spruce beetle overcome the tree's defenses. In an experiment with Sitka spruce, *C. rufipenni* was found to be three to nine times more pathogenic [*Solheim and Safranyik*, 1997].

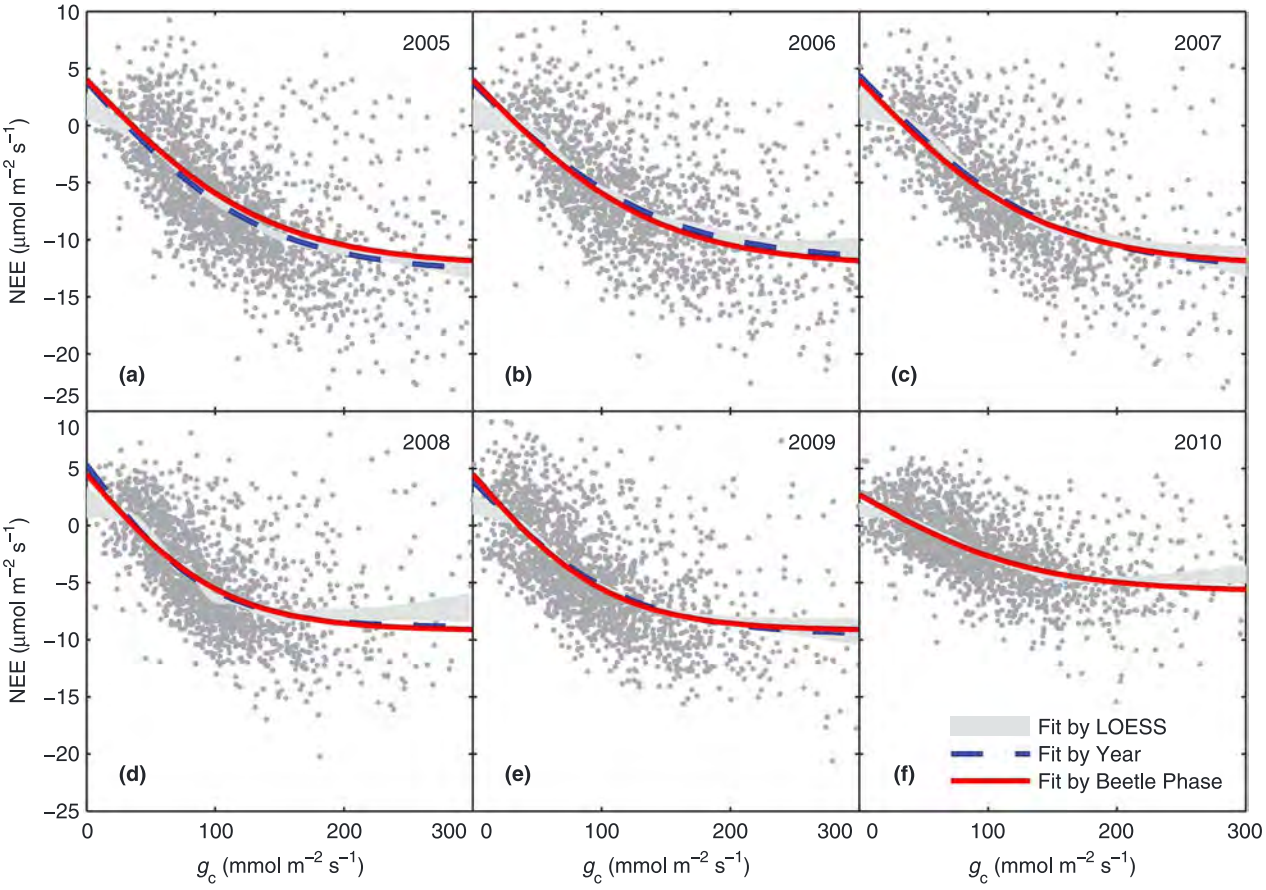

Figure 8. NEE response to canopy conductance (g_c) for daytime growing season modeled with locally weighted regression (LOESS, 95% confidence limit) and with a logistic sigmoid function (equation (2)) fit by year and by the three phases of the beetle outbreak: (a–c) endemic, (d and e) epidemic I, and (f) epidemic II. Parameters for the logistic sigmoid plots were estimated without autoregression.

The change in the g_c response to its environmental drivers was consistent with response to drought or hydraulic limitation as shown with sap flux data (Figure 3a). Engelmann spruce reduce their needle conductance in response to drought [*Brodersen et al.*, 2006; *Kaufmann*, 1979]. Stomatal conductance, light (the most significant driver), and photosynthesis are all interconnected [*Sharkey and Raschke*, 1981] such that hydraulic failure can signal a reduction in photosynthesis as observed in other conifers found in the Rocky Mountains [*Hubbard et al.*, 2001]. Thus, the 14% decrease in the g_c response to PPFD during epidemic I (Table 2) may reflect a reduction in photosynthesis from limited gas exchange due to sapwood occlusion and hydraulic failure. The 9% decrease in epidemic II was not significant (Table 2) but may have been confounded by the g_c response to $T_{s,\text{shallow}}$ (the third most significant driver); a model maintaining the $T_{s,\text{shallow}}$ parameter constant with time produced similar R^2 but the PPFD response significantly decreased 12% in epidemic II (analysis not shown). This interaction with $T_{s,\text{shallow}}$ probably occurred because the average daily $T_{s,\text{shallow}}$ decreased differently during epidemic I (−1.2°C) and II (−0.6°C) (analysis not shown) although it is possible those differences were related to changes in soil moisture (Figure 5). While it is debatable why the response to soil temperature changed throughout the epidemic, nevertheless, $T_{s,\text{shallow}}$ did affect roots and g_c. *Delucia* [1986] found that conductance in Engelmann spruce declined sharply below 8°C at a rate of about 5% °C^{-1}, while we observed average daily $T_{s,\text{shallow}}$ of 8.1°C, and the normalized (divided by average g_c) slope of the $T_{s,\text{shallow}}$ response was 6% °C^{-1} (Table 1). The change in the $T_{s,\text{shallow}}$ response over time (Table 2) could have been an artifact of the change in mean soil temperature, but we cannot rule out that root physiology changed in impacted spruce. The g_c response to VPD (the second most significant driver) did not change during the epidemic (Table 2). As spruce age, they are among a few plants whose stomatal response to VPD is less tightly regulated to plant hydraulics [*Ewers et al.*, 2005], allowing for low leaf water potentials and leading to morphological changes of higher leaf area to sapwood area ratio [*Ewers et al.*, 2005; *McDowell et al.*, 2002].

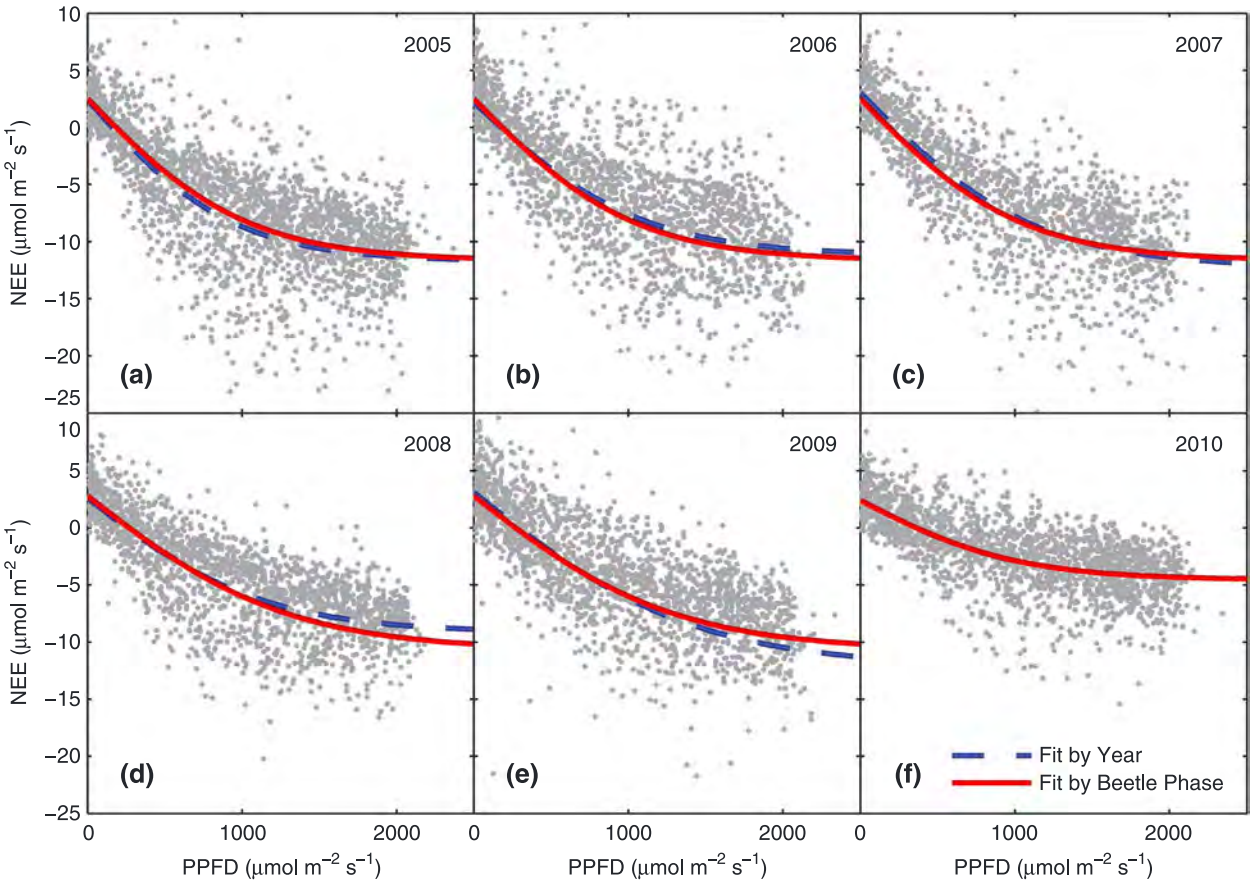

Figure 9. Net ecosystem exchange of CO_2 (NEE) response to photosynthetic photon flux density (PPFD) for daytime growing season using the logistic sigmoid (equation (4)) modeled by year and for the three phases of the beetle outbreak: (a–c) endemic, (d and e) epidemic I, and (f) epidemic II. Model parameters are in Tables 1 and 2. The response to vapor pressure deficit (VPD) was included as a constant.

If stomatal response to VPD was critical to prevent hydraulic failure in this ecosystem, then as the composition of the canopy transitioned during the epidemic from old spruce to young and small spruce and fir, the g_c response to VPD should have become more sensitive, which is the case for trees with higher reference conductance (Figure 3a). One explanation for this result is that GLEES is not a strongly water-limited system. Even though soil moisture increased throughout the epidemic (Figure 5), neither shallow nor deep soil moisture had an influence on g_c, though the influence of leaf and soil water potential on g_c is unknown.

Summer ET was reduced during the beetle epidemic despite higher precipitation and soil moisture and nearly constant average measured net and modeled diffuse radiation (analysis not shown), suggesting that the decline in summer ET was not related to precipitation. In 2005, ET remained high even with extremely low precipitation (Figures 4 and 7). More moisture was available to the ecosystem during the epidemic years when winter precipitation, summer θ_{deep}, and early summer $\theta_{shallow}$ were consistently higher (Figures 4 and 5). We found that the environmental drivers associated with the canopy conductance terms in the Penman-Monteith equation best explained the ET data, where the ET response to PPFD decreased 18% due to the beetle epidemic (Table 2 and Figure 7). Though this decline is less than the 22% decrease in the ET versus PET relationship, it was probably confounded by allowing the $T_{s,shallow}$ parameter to change over time; a model holding it constant produced similar R^2 plus a 23% reduction in the PPFD response (analysis not shown). Although VPD was a clear driver of g_c, it had no obvious relationship with ET. We did not include $\theta_{shallow}$ and θ_{deep} in our analysis because we based it on the Penman-Monteith equation. There was a correlation between ET and deep soil moisture (analysis not shown) which we conclude could have been caused by the decline in ET but not the increase in available soil water. Overall, the daily average ET decreased at GLEES during the epidemic (Figure 6) which was the equivalent of decreasing cumulative summer ET from 251 to 210 mm over

the growing season. Though the magnitude of this decrease is only 3% of the average annual precipitation at GLEES, the epidemic years did receive over 18% more precipitation. Interannual climate variability likely influenced the total amounts of cumulative summer ET; yet because we found (1) mechanistic changes in g_c and the ET response to light that corresponded to the epidemic while (2) precipitation and soil moisture increased, net and diffuse radiation remained constant, and ET decreased, we rule out climate variability as the fundamental underlying mechanism that explains the reduction in ET over time. Thus, it is possible that extra water was available to increase streamflow after the bark beetle outbreak. This has been postulated and debated [*Bewley et al.*, 2010; *Biederman et al.*, 2014; *Pugh and Gordon*, 2013] and observed over decades following previous spruce beetle outbreaks in the Rocky Mountains [*Bethlahmy*, 1974; *Bethlahmy*, 1975; *Love*, 1955]. While we cannot conclude that streamflow increased at GLEES, the observed decrease in summer ET is at least consistent with this hypothesis and warrants further investigation.

4.2. Changes in NEE

The fundamental photosynthetic biochemistry of the ecosystem did not change until the majority of the canopy finally died during epidemic II. During epidemic I, the ecosystem was fixing carbon at the same rate relative to conductance as it had in the endemic years, and that did not change until the third year of the epidemic (Tables 1 and 2, and Figure 8). We interpret this as during epidemic I, the spruce needles lived in severe drought stress because of beetle-induced hydraulic failure and reduced their stomatal conductance [*Brodersen et al.*, 2006; *Kaufmann*, 1979] and their photosynthesis [*Hubbard et al.*, 2001], all of which are fundamentally interconnected [*Katul et al.*, 2003; *Katul et al.*, 2009]. The ability of Engelmann spruce to survive for several years after catastrophic hydraulic failure is remarkable. Experiments in the Rocky Mountains found that lodgepole pine die within 1 year when xylem is occluded by blue-stain fungi [*Hubbard et al.*, 2013; *Knight et al.*, 1991]. Engelmann spruce appears more resilient. Their tree ring production can stop 1 to 3 years before they lose their green foliage and die [*Mast and Veblen*, 1994]. We also observed this phenomenon at GLEES. In our dendrochronological survey, a majority of spruce stopped growing by 2008 (Figure 1) but the canopy retained a similar green shade during epidemic I (Figures 2a versus 2b and 2c) while the slope of the NEE to g_c relationship did not change (Table 2 and Figure 8). Where the trees store carbon during this time is unknown, because bark beetles consume the cambium and effectively girdle the tree while the blue stain fungi block water flow which will also reduce sugar utilization and phloem transport [*Sevanto et al.*, 2014]. We thus speculate that carbon remains in and near the needles. But widespread spruce mortality did occur during epidemic II when the slope of the NEE to g_c relationship fell by 46% (Table 2 and Figure 8) and the canopy lost much of its green foliage (Figures 2a–2c versus 2d).

The spruce beetle disturbance had a profound impact on the NEE fluxes of CO_2. The beetle outbreak caused reductions in the magnitude of NEE during epidemic I (-24% for Φ, -8% for Φ_{direct}, and -19% for $\Phi_{diffuse}$) that further decreased during phase II (-50% for Φ, -51% for A_{max}, -56% for Φ_{direct}, and -41% for $\Phi_{diffuse}$) (logistic sigmoid in Table 2 and Figure 9). Our light response curve analysis (equation (4)) controls for the main environmental variables that influence NEE; any changes in the parameters thus reflect a more mechanistic change in the ecosystem. Because the major trends corresponded (1) to the timing of the epidemic and (2) to a soil moisture regime that actually increased, we rule out interannual climate variability as the explanation of the underlying decline in the magnitude NEE.

We did not observe a decrease in ecosystem respiration, as determined by fitting a light response curve to daytime NEE data (logistic sigmoid in Table 2 and Figure 9). Though the meaning and interpretation of ecosystem respiration derived from daytime versus nighttime eddy covariance data are not identical, they are very much related [*Lasslop et al.*, 2010]. Yet our ability to interpret ecosystem respiration dynamics from R_d alone is limited. Compared to lodgepole pine forest impacted by mountain pine beetle, one might have predicted that ecosystem respiration would have decreased [*Moore et al.*, 2013]; this does not appear to be the case in a spruce-fir forest. One explanation could be that the contribution of soil dominates total ecosystem respiration, such that the loss of spruce canopy had a minimal impact. Also, considering that spruce needles take several years to die after beetle attack, we must weigh the possibility that their roots might survive even longer, leading to stable soil respiration rates. Speckman et al. (manuscript in preparation, 2014) thoroughly investigate ecosystem respiration dynamics during the course of the GLEES epidemic by comparing nighttime eddy covariance versus chamber measurements.

There were two distinct stages of the NEE response to the epidemic which affected the carbon balance of the ecosystem. The average growing season cumulative NEE was reduced from −190 to −100 g C m^{-2} during epidemic I and then to near 0, or carbon neutral, during epidemic II (Figure 6b). It is safe to conclude that because the ecosystem was not a carbon sink during the summer, that by 2010, the subalpine forest was operating as an annual carbon source.

Our results fit within other eddy covariance studies following disturbance. In lodgepole pine forests infested with mountain pine beetle (>84% trees impacted), Φ was 25–35% lower in a stand 1–4 years after attack compared to another 4–7 years after an outbreak, while the growing season (May–September) cumulative NEE averaged −50 g C m^{-2} with some recovery of the carbon sink over time [*Brown et al.*, 2012]. A decade after a stand replacing fire in a ponderosa pine forest, NEE was still reduced (−9 to −23% for Φ_{direct} (clear), −38 to −51% for $\Phi_{diffuse}$ (cloudy), −68% to −82% for A_{max}) while the ecosystem functioned as an annual carbon source [*Dore et al.*, 2012; *Dore et al.*, 2008]. Yet in a nearby mechanical thinning treatment (35% basal area removed), changes in these parameters were less detectable while the annual carbon sink recovered within 3 years [*Dore et al.*, 2012]. The impacts on deciduous forests can be very different; in an aspen/birch girdling experiment (39% basal area affected), Φ was higher after treatment leading to a stable carbon sink [*Gough et al.*, 2013].

4.3. Meta-analysis

The declining ET and NEE fluxes are consistent with the spruce beetle impact on forest structure. For an ecosystem to have produced the observed parameter changes between the endemic and epidemic II years, it must have had (1) greater overstory than understory fluxes, (2) greater transpiration than evaporation, and (3) at least 50% loss of overstory (Table S4 and Figures S3a–S3c). Each of these appears reasonable. While *Bradford et al.* [2008] determined the understory carbon pool at GLEES to be negligible, they estimated the understory and overstory carbon fluxes to be similar. Second, at Niwot Ridge, 159 km south of GLEES in the Rocky Mountains, summer transpiration accounted for 20%–60% of ET [*Moore et al.*, 2008]. And finally, 52% of the trees at GLEES accounting for 77% of the forests basal area have been impacted by spruce beetle (Speckman et al., manuscript in preparation, 2014). For example, the Bayesian analysis demonstrates that a 2:1 overstory:understory flux ratio coupled with an 80% loss of overstory is relatively probable (Figure S3d) while being consistent with *Bradford et al.* [2008] and Speckman et al. (manuscript in preparation, 2014). Plants account for a majority of the summer vapor flux at GLEES, with the most probable transpiration: evaporation ratio being 2.5:1 (Figure S3c).

The Bayesian hierarchical model also successfully reconciled the numerous model parameters in Tables 2 and S3 into a generalized diminishment in ET and NEE. Though the boundary layer resistance of *Massman et al.* [1994] led to a low estimate of the decline in ET, the reconciled decline was not significantly difference between epidemic I and II (Table S4). And while the posterior densities have much greater uncertainty than any of the individual parameters, it is a powerful statement to summarize this study as ET declined 28 ± 4% to 36 ± 4% from epidemic I to II while simultaneously the magnitude of NEE decreased 13 ± 7% to 51 ± 4% and clearly illustrates the role of tree physiology in ecosystem responses as suggested by hypothesis b.

4.4. Can Mortality Explain Declining Fluxes Without Including Tree Physiology?

The diminishments in ET and NEE from epidemic I to II cannot be adequately described by the observable mortality alone. Had hypothesis a been supported, we would have observed simultaneous decreases in g_c, ET, and NEE that corresponded to reduced LAI and mortality. Instead, we observed temporal changes in these ecosystem fluxes that corresponded to two distinct events: (1) hydraulic failure in trees shortly after being attacked with blue-stain fungi (decline in g_c and ET) causing restricted gas exchange (diminishment in NEE) followed by (2) mortality of impacted trees (further diminishment in NEE). Thus, we reject hypothesis a in favor of hypothesis b. This is not to say that quantifying mortality is not important; our meta-analysis based on the change from the endemic to epidemic II years demonstrates a connection between post-mortality change in forest structure and the decline in ecosystem fluxes. But the dynamics of the disturbance that occurred during epidemic I cannot be explained by mortality alone, but rather by incorporating the physiological response of attacked and subsequently dying trees.

This is not the first study to attempt to explain ecosystem response to disturbance starting from the point of view of plant response [*Gough et al.*, 2013]. Why, then, does this work at our site while it fails at others? We

suggest it is because spruce-fir is a very slow response ecosystem [*Aplet et al.*, 1988] where the reallocation of resources and release of surviving trees after disturbance happen slowly, on the order of 5–15 years [*Veblen et al.*, 1991]. Thus, even though Engelmann spruce die much more slowly from spruce beetle [*Mast and Veblen*, 1994] than, for example, lodgepole pine from mountain pine beetle [*Hubbard et al.*, 2013], the entire mortality event still occurs much faster than any of the feedbacks in the spruce-fir ecosystem.

Acknowledgments

We thank John Korfmacher, Alan Ellsworth, Bob Musselman, Mage Skordahl, Heather Speckman, and the countless others who have helped at the GLEES AmeriFlux site over the past decade; John Popp for his work on the dendrochronological survey; Faith Whitehouse for the leaf assimilation data; Jason Stoker and Scott Peckham for assistance with the MODIS data; and Scott Baggett and Ben Bird for their statistical expertise. This work was funded by the U.S. Forest Service, Rocky Mountain Research Station with additional funding from the Wyoming Water Development Commission and USGS.

References

Adams, H. D., M. Guardiola-Claramonte, G. A. Barron-Gafford, J. C. Villegas, D. D. Breshears, C. B. Zou, P. A. Troch, and T. E. Huxman (2009), Temperature sensitivity of drought-induced tree mortality portends increased regional die-off under global-change-type drought, *Proc. Natl. Acad. Sci. U.S.A.*, *106*(17), 7063–7066.

Adams, H. D., C. H. Luce, D. D. Breshears, C. D. Allen, M. Weiler, V. C. Hale, A. M. S. Smith, and T. E. Huxman (2012), Ecohydrological consequences of drought- and infestation- triggered tree die-off: Insights and hypotheses, *Ecohydrology*, *5*(2), 145–159.

Adelman, J. D., B. E. Ewers, and D. S. Mackay (2008), Use of temporal patterns in vapor pressure deficit to explain spatial autocorrelation dynamics in tree transpiration, *Tree Physiol.*, *28*(4), 647–658.

Allen, C. D., et al. (2010), A global overview of drought and heat-induced tree mortality reveals emerging climate change risks for forests, *For. Ecol. Manage.*, *259*(4), 660–684.

Amiro, B. D., et al. (2010), Ecosystem carbon dioxide fluxes after disturbance in forests of North America, *J. Geophys. Res.*, *115*, G00K02, doi:10.1029/2010JG001390.

Anderegg, W. R. L., J. A. Berry, D. D. Smith, J. S. Sperry, L. D. L. Anderegg, and C. B. Field (2012), The roles of hydraulic and carbon stress in a widespread climate-induced forest die-off, *Proc. Natl. Acad. Sci. U.S.A.*, *109*(1), 233–237.

Aplet, G. H., R. D. Laven, and F. W. Smith (1988), Patterns of community dynamics in Colorado Engelmann spruce-subalpine fir forests, *Ecology*, *69*(2), 312–319.

Applequist, M. B. (1958), A simple pith locator for use with off-center increment cores, *J. For.*, *56*(2), 141.

Bender, R., and L. Heinemann (1995), Fitting nonlinear-regression models with correlated errors to individual pharmacodynamic data using SAS software, *J. Pharmacokinet. Biopharm.*, *23*(1), 87–100.

Bentz, B. J., J. Regniere, C. J. Fettig, E. M. Hansen, J. L. Hayes, J. A. Hicke, R. G. Kelsey, J. F. Negron, and S. J. Seybold (2010), Climate change and bark beetles of the western United States and Canada: Direct and indirect effects, *BioScience*, *60*(8), 602–613.

Bethlahmy, N. (1974), More streamflow after a bark beetle epidemic, *J. Hydrol.*, *23*(3–4), 185–189.

Bethlahmy, N. (1975), A Colorado episode: Beetle epidemic, ghost forests, more streamflow, *Northwest Sci.*, *49*(2), 95–105.

Bewley, D., Y. Alila, and A. Varhola (2010), Variability of snow water equivalent and snow energetics across a large catchment subject to mountain pine beetle infestation and rapid salvage logging, *J. Hydrol.*, *388*(3–4), 464–479.

Biederman, J. A., P. D. Brooks, A. A. Harpold, D. J. Gochis, E. Gutmann, D. E. Reed, E. Pendall, and B. E. Ewers (2014), Multiscale observations of snow accumulation and peak snowpack following widespread, insect-induced lodgepole pine mortality, *Ecohydrology*, *7*, 150–162.

Bradford, J. B., R. A. Birdsey, L. A. Joyce, and M. G. Ryan (2008), Tree age, disturbance history, and carbon stocks and fluxes in subalpine Rocky Mountain forests, *Global Change Biol.*, *14*(12), 2882–2897.

Brodersen, C. R., M. J. Germino, and W. K. Smith (2006), Photosynthesis during an episodic drought in *Abies lasiocarpa* and *Picea engelmannii* across an alpine treeline, *Arct. Antarct. Alp. Res.*, *38*(1), 34–41.

Brown, M. G., et al. (2012), The carbon balance of two lodgepole pine stands recovering from mountain pine beetle attack in British Columbia, *Agric. For. Meteorol.*, *153*, 82–93.

Brutsaert, W. (1982), *Evaporation into the Atmosphere: Theory, History, and Applications*, D. Reidel Company, Dordrecht, Netherlands.

Burba, G. G., D. K. McDermitt, A. Grelle, D. J. Anderson, and L. K. Xu (2008), Addressing the influence of instrument surface heat exchange on the measurements of CO_2 flux from open-path gas analyzers, *Global Change Biol.*, *14*(8), 1854–1876.

Campbell, G. S., and J. M. Norman (1998), *An Introduction to Environmental Biophysics*, 2nd ed., Springer-Verlang, New York.

Cleveland, W. S. (1979), Robust locally weighted regression and smoothing scatterplots, *J. Am. Stat. Assoc.*, *74*(368), 829–836.

Cleveland, W. S., and S. J. Devlin (1988), Locally weighted regression: An approach to regression analysis by local fitting, *J. Am. Stat. Assoc.*, *83*(403), 596–610.

Cottam, G., and J. T. Curtis (1956), The use of distance measures in phytosociological sampling, *Ecology*, *37*(3), 451–460.

Delucia, E. H. (1986), Effect of low root temperature on net photosynthesis, stomatal conductance and carbohydrate concentration in Engelmann spruce (*Picea engelmannii* Parry ex Engelm.) seedlings, *Tree Physiol.*, *2*(1–3), 143–154.

Dore, S., M. Montes-Helu, S. C. Hart, B. A. Hungate, G. W. Koch, J. B. Moon, A. J. Finkral, and T. E. Kolb (2012), Recovery of ponderosa pine ecosystem carbon and water fluxes from thinning and stand-replacing fire, *Global Change Biol.*, *18*(10), 3171–3185.

Dore, S., T. E. Kolb, M. Montes-Helu, B. W. Sullivan, W. D. Winslow, S. C. Hart, J. P. Kaye, G. W. Koch, and B. A. Hungate (2008), Long-term impact of a stand-replacing fire on ecosystem CO_2 exchange of a ponderosa pine forest, *Global Change Biol.*, *14*(8), 1801–1820.

Dymerski, A. D., J. A. Anhold, and A. S. Munson (2001), Spruce beetle (*Dendroctonus rufipennis*) outbreak in Engelmann spruce (*Picea Engelmannii*) in central Utah, 1986-1998, *Western North Am. Naturalist*, *61*(1), 19–24.

Edburg, S. L., J. A. Hicke, P. D. Brooks, E. G. Pendall, B. E. Ewers, U. Norton, D. Gochis, E. D. Gutmann, and A. J. H. Meddens (2012), Cascading impacts of bark beetle-caused tree mortality on coupled biogeophysical and biogeochemical processes, *Frontiers Ecol. Environ.*, *10*(8), 416–424.

Ewers, B. E., S. T. Gower, B. Bond-Lamberty, and C. K. Wang (2005), Effects of stand age and tree species on canopy transpiration and average stomatal conductance of boreal forests, *Plant Cell Environ.*, *28*(5), 660–678.

Finnigan, J. (2008), An introduction to flux measurements in difficult conditions, *Ecol. Appl.*, *18*(6), 1340–1350.

Foken, T., M. Göockede, M. Mauder, L. Mahrt, B. Amiro, and W. Munger (2004), Post-field data quality control, in *Handbook of Micrometeorology*, edited by X. Lee, W. J. Massman, and B. E. Law, pp. 181–208, Kluwer Academic Publishers, Dordrecht, The Netherlands.

Gash, J. H. C. (1986), A note on estimating the effect of a limited fetch on micrometeorological evaporation measurements, *Boundary Layer Meteorol.*, *35*(4), 409–413.

Gelman, A., J. B. Carlin, H. S. Stern, and D. B. Rubin (2004), *Bayesian Data Analysis*, 2nd ed., 668 pp., Chapman & Hall/CRC Press, Boca Raton, Fla.

Gough, C. M., B. S. Hardiman, L. Nave, G. Bohrer, K. D. Maurer, C. S. Vogel, K. J. Nadelhoffer, and P. S. Curtis (2013), Sustained carbon uptake and storage following moderate disturbance in a Great Lakes forest, *Ecol. Appl.*, *23*(5), 1202–1215.

Granier, A. (1987), Evaluation of transpiration in a Douglas-fir stand by means of sap flow measurements, *Tree Physiol.*, *3*(4), 309–320.

Gu, L., W. J. Massman, R. Leuning, S. G. Pallardy, T. Meyers, P. J. Hanson, J. S. Riggs, K. P. Hosman, and B. Yang (2012), The fundamental equation of eddy covariance and its application in flux measurements, *Agric. For. Meteorol.*, *152*, 135–148.
Gu, L. H., et al. (2005), Objective threshold determination for nighttime eddy flux filtering, *Agric. For. Meteorol.*, *128*(3–4), 179–197.
Hansen, E. M., and B. J. Bentz (2003), Comparison of reproductive capacity among univoltine, semivoltine, and re-emerged parent spruce beetles (Coleoptera: Scolytidae), *Can. Entomologist*, *135*(05), 697–712.
Hochberg, Y., and A. C. Tamhane (1987), *Multiple Comparison Procedures*, Wiley, New York.
Højstrup, J. (1993), A statistical-data screening-procedure, *Meas. Sci. Technol.*, *4*(2), 153–157.
Horst, T. W. (1997), A simple formula for attenuation of eddy fluxes measured with first-order-response scalar sensors, *Boundary Layer Meteorol.*, *82*(2), 219–233.
Horst, T. W., and D. H. Lenschow (2009), Attenuation of scalar fluxes measured with spatially-displaced sensors, *Boundary Layer Meteorol.*, *130*(2), 275–300.
Hubbard, R. M., M. G. Ryan, V. Stiller, and J. S. Sperry (2001), Stomatal conductance and photosynthesis vary linearly with plant hydraulic conductance in ponderosa pine, *Plant Cell Environ.*, *24*(1), 113–121.
Hubbard, R. M., C. C. Rhoades, K. Elder, and J. Negron (2013), Changes in transpiration and foliage growth in lodgepole pine trees following mountain pine beetle attack and mechanical girdling, *For. Ecol. Manage.*, *289*, 312–317.
Jarvis, P. G. (1976), The interpretation of the variations in leaf water potential and stomatal conductance found in canopies in the field, *Philos. Trans. R. Soc. London B Biol. Sci.*, *273*(927), 593–610.
Jarvis, P. G. (1995), Scaling processes and problems, *Plant Cell Environ.*, *18*(10), 1079–1089.
Kaimal, J. C., and J. J. Finnigan (1994), *Atmospheric Boundary Layer Flows: Their Structure and Measurement*, Oxford Univ. Press, New York.
Katul, G., R. Leuning, and R. Oren (2003), Relationship between plant hydraulic and biochemical properties derived from a steady-state coupled water and carbon transport model, *Plant Cell Environ.*, *26*(3), 339–350.
Katul, G. G., S. Palmroth, and R. A. M. Oren (2009), Leaf stomatal responses to vapour pressure deficit under current and CO_2-enriched atmosphere explained by the economics of gas exchange, *Plant Cell Environ.*, *32*(8), 968–979.
Kaufmann, M. R. (1979), Stomatal control and the development of water deficit in Engelmann spruce seedlings during drought, *Can. J. For. Res.*, *9*(3), 297–304.
Knight, D. H., J. B. Yavitt, and G. D. Joyce (1991), Water and nitrogen outflow from lodgepole pine forest after two levels of tree mortality, *For. Ecol. Manage.*, *46*(3–4), 215–225.
Lasslop, G., M. Reichstein, D. Papale, A. D. Richardson, A. Arneth, A. Barr, P. Stoy, and G. Wohlfahrt (2010), Separation of net ecosystem exchange into assimilation and respiration using a light response curve approach: Critical issues and global evaluation, *Global Change Biol.*, *16*(1), 187–208.
Lee, X., and W. J. Massman (2011), A perspective on thirty years of the Webb, Pearman and Leuning density corrections, *Boundary Layer Meteorol.*, *139*(1), 37–59.
Lee, X., J. J. Finnigan, and K. T. Paw U (2004a), Coordinate system and flux bias error, in *Handbook of Micrometeorology*, edited by X. Lee, W. J. Massman, and B. E. Law, pp. 33–66, Kluwer Academic Publishers, Dordrecht, The Netherlands.
Lee, X., W. J. Massman, and B. E. Law (2004b), *Handbook of Micrometeorology*, Kluwer Academic Publishers, Dordrecht, The Netherlands.
Loescher, H. W., C. V. Hanson, and T. W. Ocheltree (2009), The psychrometric constant is not constant: A novel approach to enhance the accuracy and precision of latent energy fluxes through automated water vapor calibrations, *J. Hydrometeorol.*, *10*(5), 1271–1284.
Long, S. P., and C. J. Bernacchi (2003), Gas exchange measurements, what can they tell us about the underlying limitations to photosynthesis? Procedures and sources of error, *J. Exp. Bot.*, *54*(392), 2393–2401.
Love, L. D. (1955), The effect on stream flow of the killing of spruce and pine by the Engelmann spruce beetle, *Trans. Am. Geophys. Union*, *36*(1), 113–118.
Mackay, D. S., D. E. Ahl, B. E. Ewers, S. T. Gower, S. N. Burrows, S. Samanta, and K. J. Davis (2002), Effects of aggregated classifications of forest composition on estimates of evapotranspiration in a northern Wisconsin forest, *Global Change Biol.*, *8*(12), 1253–1265.
Masek, J. G., C. Huang, R. Wolfe, W. Cohen, F. Hall, J. Kutler, and P. Nelson (2008), North American forest disturbance mapped from a decadal Landsat record, *Remote Sens. Environ.*, *112*(6), 2914–2926.
Massman, W. J. (2000), A simple method for estimating frequency response corrections for eddy covariance systems, *Agric. For. Meteorol.*, *104*(3), 185–198.
Massman, W. J., and M. R. Kaufmann (1991), Stomatal response to certain environmental factors: a comparison of models for subalpine trees in the Rocky Mountains, *Agric. For. Meteorol.*, *54*(2–4), 155–167.
Massman, W. J., and X. Lee (2002), Eddy covariance flux corrections and uncertainties in long-term studies of carbon and energy exchanges, *Agric. For. Meteorol.*, *113*(1–4), 121–144.
Massman, W. J., and R. Clement (2004), Uncertainty in eddy covariance flux estimates resulting from spectral attenuation, in *Handbook of Micrometeorology*, edited by X. Lee, W. J. Massman, and B. E. Law, pp. 67–99, Kluwer Academic Publishers, Dordrecht, The Netherlands.
Massman, W. J., J. Pederson, A. Delany, D. Grantz, G. Denhartog, H. H. Neumann, S. P. Oncley, R. Pearson, and R. H. Shaw (1994), An evaluation of the regional acid deposition model surface module for ozone uptake at three sites in the San Joaquin Valley of California, *J. Geophys. Res.*, *99*(D4), 8281–8294, doi:10.1029/93JD03267.
Mast, J. N., and T. T. Veblen (1994), A dendrochronological method of studying tree mortality patterns, *Phys. Geogr.*, *15*(6), 529–542.
McCambridge, W. F., and F. B. Knight (1972), Factors affecting spruce beetles during a small outbreak, *Ecology*, *53*(5), 830–839.
McDowell, N. M., et al. (2002), The relationship between tree height and leaf area: Sapwood area ratio, *Oecologia*, *132*(1), 12–20.
Meek, D. W., J. H. Prueger, and T. J. Sauer (1998), Solutions for three regression problems commonly found in meteorological data analysis, paper presented at 23rd Conference on Agricultural Forest Meteorology, American Meteorological Society, Albuquerque, NM, November 2–7, 1998.
Miller, L. K., and R. A. Werner (1987), Cold-hardiness of adult and larval spruce beetles *Dendroctonus rufipennis* (Kirby) in interior Alaska, *Can. J. Zool.*, *65*(12), 2927–2930.
Moffat, A. M. (2010), A new methodology to interpret high resolution measurements of net carbon fluxes between the terrestrial ecosystems and the atmosphere, Doctoral thesis, Friedrich Schiller University, Jena.
Monteith, J. L., and M. H. Unsworth (2008), *Principles of Environmental Physics*, 3rd ed., Academic Press, Burlington, Mass.
Moore, D. J. P., J. Hu, W. J. Sacks, D. S. Schimel, and R. K. Monson (2008), Estimating transpiration and the sensitivity of carbon uptake to water availability in a subalpine forest using a simple ecosystem process model informed by measured net CO_2 and H_2O fluxes, *Agric. For. Meteorol.*, *148*(10), 1467–1477.
Moore, D. J. P., N. A. Trahan, P. Wilkes, T. Quaife, B. B. Stephens, K. Elder, A. R. Desai, J. Negron, and R. K. Monson (2013), Persistent reduced ecosystem respiration after insect disturbance in high elevation forests, *Ecol. Lett.*, *16*(6), 731–737.

Musselman, R. C. (1994), The Glacier Lakes Ecosystem Experiments Site, USDA Forest Service, Rocky Mountain Forest and Range Experiment Station, General Technical Report RM–249.
Myneni, R. B., et al. (2002), Global products of vegetation leaf area and fraction absorbed PAR from year one of MODIS data, *Remote Sens. Environ.*, *83*(1–2), 214–231.
Natural Resources Canada (2010), Statistical data – Canada's forests, [Available at http://canadaforests.nrcan.gc.ca/statsprofile/forest/ca, accessed July 25, 2012.
Oren, R., N. Phillips, B. E. Ewers, D. E. Pataki, and J. P. Megonigal (1999), Sap-flux-scaled transpiration responses to light, vapor pressure deficit, and leaf area reduction in a flooded *Taxodium distichum* forest, *Tree Physiol.*, *19*(6), 337–347.
Paine, T. D., K. F. Raffa, and T. C. Harrington (1997), Interactions among scolytid bark beetles, their associated fungi, and live host conifers, *Annu. Rev. Entomol.*, *42*(1), 179–206.
Pataki, D. E., R. Oren, and W. K. Smith (2000), Sap flux of co-occurring species in a western subalpine forest during seasonal soil drought, *Ecology*, *81*(9), 2557–2566.
Penman, H. L. (1948), Natural evaporation from open water, bare soil and grass, *Proc. R. Soc. London Ser. A Math. Phys. Sci.*, *193*(1032), 120–145.
Piepho, H.-P. (2004), An Algorithm for a Letter-Based Representation of All-Pairwise Comparisons, *J. Comput. Graph. Stat.*, *13*(2), 456–466.
Pugh, E., and E. Gordon (2013), A conceptual model of water yield effects from beetle-induced tree death in snow-dominated lodgepole pine forests, *Hydrol. Process.*, *27*(14), 2048–2060.
Raffa, K. F., B. H. Aukema, B. J. Bentz, A. L. Carroll, J. A. Hicke, M. G. Turner, and W. H. Romme (2008), Cross-scale drivers of natural disturbances prone to anthropogenic amplification: The dynamics of bark beetle eruptions, *BioScience*, *58*(6), 501–517.
Rubin, D. B. (1981), Estimation in parallel randomized experiments, *J. Educational Stat.*, *6*(4), 377–401.
Schmid, J. M., and R. H. Frye (1977), Spruce beetle in the Rockies, USDA, RM-49.
Sellers, P. J., et al. (1997), BOREAS in 1997: Experiment overview, scientific results, and future directions, *J. Geophys. Res.*, *102*(D24), 28,731–28,769.
Sevanto, S., N. G. McDowell, L. T. Dickman, R. Pangle, and W. T. Pockman (2014), How do trees die? A test of the hydraulic failure and carbon starvation hypotheses, *Plant Cell Environ.*, *37*(1), 153–161.
Sharkey, T. D., and K. Raschke (1981), Separation and measurement of direct and indirect effects of light on stomata, *Plant Physiol.*, *68*(1), 33–40.
Six, D. L., and B. J. Bentz (2003), Fungi associated with the North American spruce beetle, *Dendroctonus rufipennis*, *Can. J. For. Res.*, *33*(9), 1815–1820.
Solheim, H., and L. Safranyik (1997), Pathogenicity to Sitka spruce of *Ceratocystis rufipenni* and *Leptographium abietinum* blue-stain fungi associated with the spruce beetle, *Can. J. For. Res.*, *27*(9), 1336–1341.
Spitters, C. J. T., H. Toussaint, and J. Goudriaan (1986), Separating the diffuse and direct component of global radiation and its implications for modeling canopy photosynthesis. Part I. Components of incoming radiation, *Agric. For. Meteorol.*, *38*(1–3), 217–229.
Stokes, M. A., and T. L. Smiley (1968), *An Introduction to Tree-Ring Dating*, Univ. of Chicago Press, Chicago, Ill.
Thom, A. S., and H. R. Oliver (1977), On Penman's equation for estimating regional evaporation, *Q. J. R. Meteorol. Soc.*, *103*(436), 345–357.
USDA Forest Service (2009), Major forest insect and disease conditions in the United States 2007, USDA Forest Service, FS-919.
USDA Forest Service (2012), Major forest insect and disease conditions in the United States: 2010 update, USDA Forest Service, FS-988.
van Mantgem, P. J., et al. (2009), Widespread increase of tree mortality rates in the western United States, *Science*, *323*(5913), 521–524.
Veblen, T. T., K. S. Hadley, M. S. Reid, and A. J. Rebertus (1991), The response of subalpine forests to spruce beetle outbreak in Colorado, *Ecology*, *72*(1), 213–231.
Vickers, D., and L. Mahrt (1997), Quality control and flux sampling problems for tower and aircraft data, *J. Atmos. Oceanic Technol.*, *14*(3), 512–526.
Webb, E. K., G. I. Pearman, and R. Leuning (1980), Correction of flux measurements for density effects due to heat and water vapour transfer, *Q. J. R. Meteorol. Soc.*, *106*(447), 85–100.
Wingfield, M. J., T. C. Harrington, and H. Solheim (1997), Two species in the *Ceratocystis coerulescens* complex from conifers in western North America, *Can. J. Bot.*, *75*(5), 827–834.
Yamaoka, Y., R. H. Swanson, and Y. Hiratsuka (1990), Inoculation of lodgepole pine with four blue-stain fungi associated with mountain pine beetle, monitored by a heat pulse velocity (HPV) instrument, *Can. J. For. Res.*, *20*(1), 31–36.
Yamaoka, Y., Y. Hiratsuka, and P. J. Maruyama (1995), The ability of *Ophiostoma clavigerum* to kill mature lodgepole pine trees, *Eur. J. For. Pathol.*, *25*(6–7), 401–404.